



Dynamic analysis of flat and folded laminated composite plates under hygrothermal environment using a nonpolynomial shear deformation theory

Babu Ranjan Thakur*, Surendra Verma, B.N. Singh, D.K. Maiti

Department of Aerospace Engineering, Indian Institute of Technology Kharagpur, W. Bengal 721302, India



ARTICLE INFO

Keywords:

Dynamic analysis
Hygrothermal environment
Folded plate
Finite element method
Nonpolynomial shear deformation theory
(NPSDT)

ABSTRACT

In this paper, the effect of the hygrothermal environment on the dynamic analysis of one-fold and two-fold folded laminated composite plates using a nonpolynomial shear deformation theory (NPSDT) is investigated. A computationally efficient C^0 finite element method (FEM) is applied to examine the free vibration characteristic, transient behavior, and steady-state response of laminated composite plates. The formulation employs the total Lagrangian approach for analysis, and the initial stress generated due to hygrothermal load is taken into account through the Green–Lagrange strain displacement relation. The Newmark's method is employed to integrate the spatial–temporal partial differential governing equations. The effect of the thermal environment on the natural frequency of folded and flat composite plates has been illustrated through various examples. The transient displacement and stresses are plotted for various loads. Moreover, transient damped analysis under the thermal load is carried out by considering the Rayleigh damping model. Further, linear harmonic analysis under the hygrothermal environment has also been carried out, and the responses in the neighborhood of natural frequency are plotted. The present model has been compared and validated by the existing literature and the obtained ANSYS APDL solutions, and is found to be performing better for NPSDT.

1. Introduction

The advent of advanced composite materials has brought a paradigm shift in the structural design and manufacturing of aircraft, automobiles, ships, etc. Especially, aerospace and structural application are the biggest beneficiaries of this development. The reason can be attributed to the low density, high strength, and high stiffness of the composite structure. Further, for the holistic analysis of structural engineering, different types of structures like flat and folded plates are needed to be considered. As these types of structures are often used in aircraft fuselages, winglets, vehicle chassis, ship hulls, buildings, bridges, etc. Besides, the folded structures are observed in nature as well, such as palm leaves, seashells, etc. In addition, the composite structures used in these applications undergo large variations in the hygrothermal environment due to their manufacturing process and operation. Moreover, the hygrothermal environment profoundly affects the behavior of composite material due to the greater susceptibility of the matrix than the fiber under the elevated hygrothermal environment. Due to this, the transverse direction displacement is more in the matrix than the fiber, which seeks for the relative move-

ment of a constituent, and the same is restricted due to different properties of the fiber and matrix. This leads to the development of induced hygrothermal residual stress. Often, these stresses induce large deformation and need to be considered for structural analysis. Also, it has been observed that the elastic modulus and the strength of composite laminates degrade at elevated temperatures. And hence, it is imperative to make a proper assessment of the thermal and moisture effect on the structure to have proper design and analysis to safeguard the structural life.

Further, the transverse shear deformation is an inherent characteristic found in the multilayered composite structure and therefore needs to be taken care of during the analysis. To incorporate this, several shear deformation theories have been proposed by various researchers as can be found in the review paper of Ghugal and Shimpi [1]. These theories can be classified as polynomial shear deformation theory (PSDT) and nonpolynomial shear deformation theory (NPSDT). The polynomial theories are obtained by considering few terms of Taylor's series for the kinematic equation, and the nonpolynomial theories take nonpolynomial functions to model the kinematic equation properly. It is observed that the polynomial shear deformation theories do not reg-

* Corresponding author.

E-mail addresses: brt.iitkgp@gmail.com, brtjsk@iitkgp.ac.in (B.R. Thakur), surendraverma2501@gmail.com (S. Verma), bnsingh@aero.iitkgp.ernet.in (B.N. Singh), dkmaiti@aero.iitkgp.ernet.in (D.K. Maiti).

ister an increase in accuracy with an increase in the order of the polynomial after the third order. On the other hand, the nonpolynomial shear deformation theories give a wide range of scope to look for an increase in accuracy [2]. There are several research works available utilizing nonpolynomial shear deformation theory. For example, Gupta and Ghosh [3] studied the static and dynamic analysis of composite plate using nonpolynomial shear deformation theory. And the same theory is also utilized by Thakur et al. [4] for the geometrically nonlinear dynamic analysis of a laminated composite plate structure. Further, as per the author's knowledge, very few have studied the structural response under the hygrothermal environment using a nonpolynomial shear deformation theory. Such as, Zenkour [5] studied the hygrothermal effects on the bending of angle-ply composite plates using a sinusoidal theory. Later, Ramos et al. [6] used the trigonometrical theory based on Carrera's unified formulation to study the laminated composite plate under thermal load. Recently, Garg et al. [7] utilized the trigonometric zigzag theory to study the static analysis of laminated composite plate under hygro-thermal-mechanical loading. However, the dynamic analysis using nonpolynomial shear deformation theories under the consideration of a hygrothermal environment has not been reported enough despite a large number of NPSDT theories that have been proposed [8]. Hence, the present work considers nonpolynomial shear deformation theory to model the kinematic of the problem for free vibration, transient vibration, and steady-state harmonic solution, under the hygrothermal environment.

Having mentioned the effect of the hygrothermal environment and the need to incorporate the shear deformation theory, the works pertaining to these are elucidated further. The initial works in this regard are mainly pertaining to the static analysis, and often deal with the transverse stress variation only, and utilize classical plate theory (CPT) [9–11]. Later, first-order shear deformation theory is utilized by several researchers [12–16] to study the dynamic characteristics of a laminated composite plate under the hygrothermal environment. Recently, a simplified plate theory to analyze vibration characteristics of the composite laminated sector, annular, and circular plate is proposed by Zhang et al. [17]. Further, higher-order polynomial shear deformation theories have also been utilized by several researchers to analyze the structural response under thermal load [18–21], however, their works are primarily limited to static and transient displacement response. Later, Zhao et al. [22] utilized the piecewise shear deformation theory in conjunction with the finite element formulation for vibration analysis of laminated composite and sandwich plates in thermal environments. Zenkour [23] investigated the Levy type solutions for deflection and stresses of a thin rectangular plate having variable thickness under the hygrothermal environment. Recently, Vinyas and Kattimani [24] used higher-order shear deformation theory in conjunction with the finite element analysis to evaluate the free vibration characteristics of a magnetoelectro-elastic rectangular plate in the hygrothermal environment. Apart from the 2D displacement finite element method, other approaches have also been employed to analyze the composite laminate under the hygrothermal environment by several researchers [25–32]; these include three-dimensional finite element method, variational asymptotic approach, etc. Recently, Cheng et al. [33] carried out an experimental study on the environmental durability of carbon/ flax fiber hybrid composite. Also, Garg and Chalak [34] have done a thorough review of the structural analysis under the hygrothermal environment. Further, the finite element solutions for the natural frequency of laminated composite structure under thermal effect have been presented by Sit and Ray [35]. In addition, several researchers have studied the behavior of a composite structure under hygrothermal environment [36–39] through various approaches, however, these works primarily confined to a limited domain of flat plate.

The literature mentioned above for the hygrothermal environment does not consider the damping modeling of the structure. However, the damping characteristic is inherent and should be analyzed accord-

ingly for a holistic understanding of the dynamic behavior of laminated composite. Several works have been reported in the literature regarding the damped dynamic analysis, such as Zabaras and Pervez [40] modeled the damping phenomena in the laminated composite by the consideration of viscous damping. Later, Pervez and Zabaras [41] used the refined plate theory to study the transient dynamic and damping analysis of laminated anisotropic plate. Further, Latheswary et al. [42] have investigated the effect of damping on transient analysis by Rayleigh damping model utilizing higher-order shear deformation theory. Recently, Assaee and Pournoori [43] studied the development of a viscoelastic spline finite strip formulation for transient analysis of plates. Pap and Kollar [44] have studied the dynamic response of the rectangular floor subjected to periodic force excitation. Moreover, Zhang et al. [45] studied the harmonic response analysis of coupled plate structures using the dynamic stiffness method. It is to be noticed that all these works above-mentioned in this paragraph consider the damping without thermal load. Nevertheless, Alijani et al. [46] have studied the linear harmonic response of functionally graded plate under hygrothermal response very briefly; apart from this, as per the author's knowledge, no other work is found for the linear damped response under hygrothermal environment.

The works pertaining to the dynamic analysis of laminated composite flat plate under hygrothermal environment have been elucidated above, now the works pertaining to the folded plate are delineated. Initial work pertaining to folded plate is done by Goldberg and Leve [47] to study the exact static analysis of folded plate structures. Later, Irie et al. [48] calculated the natural frequency of cantilever folded plates using the Ritz method. Further, several researchers investigated the folded structures by employing different approach, like finite element method [49–52], spectral element method [53], finite strip method [54–56], and transfer matrix method [57–59], etc. The mixed shell element is utilized for the folded plate and curved shell by Duan and Miyamoto [60]. Moreover, Schlothauer et al. [61] carried out the structural analysis of folded composite materials, in which usage of the outstanding flexibility of thin composite shells is carried out. Le-Anh et al. [62] utilized an adjusted differential evolution algorithm and a smoothed triangle plate element for the static and frequency optimization of folded laminated composite plates. Wang et al. [63] carried out an experimental study on the radar absorbing characteristics of folded core structures. Xiang et al. [64] studied the rectangular sandwich plates with Miura-ori folded core under quasi-static loadings. Ye et al. [65] studied the energy absorption behaviors of pre-folded composite tubes with the full diamond origami patterns. Mader et al. [66] studied bio-inspired integrated pneumatic actuation for compliant fiber-reinforced plastics. Recently, Thakur et al. [67] have studied the dynamic analysis of folded laminated composite plate structure utilizing a nonpolynomial shear deformation theory. It is to be noticed that hygrothermal load has not been considered in all these works pertaining to the folded plate. However, Das and Niyogi [68] have considered the hygrothermal load, only for the free vibration analysis of folded plate.

After an extensive survey of the available literature, it is observed that the dynamic behavior of flat and folded laminated composite is highly susceptible to the hygrothermal environment. As per the author's knowledge, however, work has not been adequately done in this field. Moreover, most of the works available in this regard are about polynomial shear deformation theory, and particularly with first-order shear deformation theory (FSDT). The transient analysis of folded laminated composite plate under hygrothermal environment has not been addressed, as per our knowledge. Further, the transient stresses of laminated composite plates under the hygrothermal environment have rarely been addressed adequately. And the damped transient response and steady-state harmonic response under hygrothermal environment are hardly observed in the literature. Hence, there is a need to extend the horizon of understanding for the dynamic behavior of flat and folded laminated composite plate

under the hygrothermal environment. Therefore, the present paper deals with the free and forced vibration of flat and folded laminated composite plate under the hygrothermal environment using a nonpolynomial shear deformation theory.

2. Mathematical formulation

To illustrate the finite element mathematical formulation for the dynamic analysis of flat and folded laminated composite plate, a rectangular laminated composite plate of dimensions, $a \times b \times h$, is considered. The plate is made up of k orthotropic layers stacked in sequence ($\Theta_1/\Theta_2/\Theta_3/\Theta_4 \dots$). The schematic diagram of a laminated composite flat plate in the Cartesian coordinate system ($X - Y - Z$) is shown in Fig. 1. First of all, the formulation pertaining to flat plate is elucidated, then the formulation concerning folded plate is presented with the use of a transformation matrix.

A nonpolynomial shear deformation theory (NPSDT), given by Grover et al. [69], has been considered for the displacement field model, as the theory in the subject is performing quite well over other theory for the static and dynamic analysis [3,67,70]. This NPSDT, also known as inverse hyperbolic shear deformation theory (IHSDT), is expressed as follows

$$\begin{aligned} u(x, y, z, t) &= u_0(x, y, t) - z \frac{\partial w_0}{\partial x} + f(z)\theta_x(x, y, t) \\ v(x, y, z, t) &= v_0(x, y, t) - z \frac{\partial w_0}{\partial y} + f(z)\theta_y(x, y, t) \\ w(x, y, z, t) &= w_0(x, y, t) \end{aligned} \quad (1)$$

where $f(z) = (g(z) + z\Omega)$, $g(z) = \sinh^{-1}(\frac{z}{h})$ and $\Omega = \frac{-2r}{h\sqrt{r^2+4}}$, $r = 3$ where, u_0 , v_0 , and w_0 are the mid-plane displacements; θ_x and θ_y are the shear deformations at the mid-plane. The parameter, r , is the transverse shear strain parameter, and h is the plate thickness. The function, $f(z)$, is the shear strain function, and the plot of the various $f(z)$ along the thickness of the plate can be observed in Ref. [69].

In Eq. (1), the displacement fields comprise the derivatives of the field variables. Hence, C^1 continuity requires to be satisfied for the finite element method. However, it is a cumbersome task to achieve C^1 continuity in FEM, therefore, by imposing an artificial constraint as $-\partial w_0/\partial x = \phi_x$, and $-\partial w_0/\partial y = \phi_y$, the requirement of C^1 continuity is reduced to C^0 continuity. So, after incorporating the artificial constraint, the new displacement field model would be

$$\begin{aligned} u(x, y, z, t) &= u_0(x, y, t) + z\phi_x + f(z)\theta_x(x, y, t) \\ v(x, y, z, t) &= v_0(x, y, t) + z\phi_y + f(z)\theta_y(x, y, t) \\ w(x, y, z, t) &= w_0(x, y, t) \end{aligned} \quad (2)$$

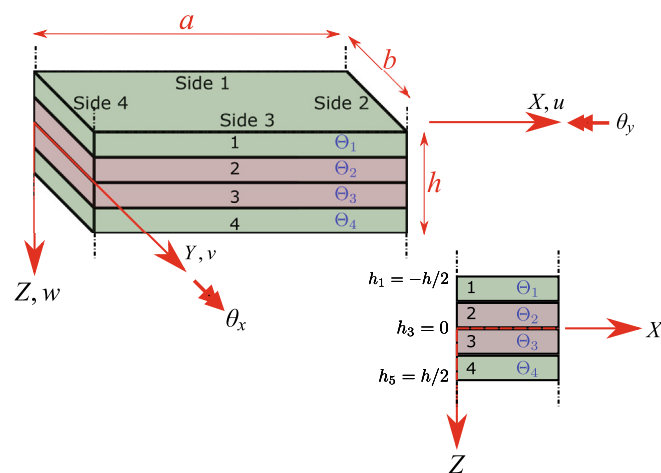


Fig. 1. Schematic diagram of laminated composite plate.

Although the linear analysis has been carried out in the present work, to calculate the initial stress stiffness, the Green–Lagrange strain displacement relation has been used. Hence, the Green–Lagrange state-of-strain, $\{\epsilon\}$ at a point corresponding to new displacement field (Eq. (2)) in the Cartesian coordinate system, is expressed as

$$\{\epsilon\} = \begin{Bmatrix} \epsilon_{xx} \\ \epsilon_{yy} \\ \gamma_{xy} \\ \gamma_{yz} \\ \gamma_{xz} \end{Bmatrix} = \begin{Bmatrix} \frac{\partial u}{\partial x} \\ \frac{\partial v}{\partial y} \\ \frac{\partial u}{\partial y} + \frac{\partial v}{\partial x} \\ \frac{\partial v}{\partial z} + \frac{\partial w}{\partial y} \\ \frac{\partial w}{\partial z} + \frac{\partial u}{\partial x} \end{Bmatrix} + \frac{1}{2} \begin{Bmatrix} (\frac{\partial u}{\partial x})^2 + (\frac{\partial v}{\partial x})^2 + (\frac{\partial w}{\partial x})^2 \\ (\frac{\partial u}{\partial y})^2 + (\frac{\partial v}{\partial y})^2 + (\frac{\partial w}{\partial y})^2 \\ 2\{\frac{\partial u}{\partial x}\frac{\partial v}{\partial y} + \frac{\partial v}{\partial x}\frac{\partial w}{\partial y} + \frac{\partial w}{\partial x}\frac{\partial u}{\partial y}\} \\ 2\{\frac{\partial u}{\partial y}\frac{\partial v}{\partial z} + \frac{\partial v}{\partial y}\frac{\partial w}{\partial z} + \frac{\partial w}{\partial y}\frac{\partial u}{\partial z}\} \\ 2\{\frac{\partial u}{\partial x}\frac{\partial w}{\partial z} + \frac{\partial v}{\partial x}\frac{\partial w}{\partial z} + \frac{\partial w}{\partial x}\frac{\partial u}{\partial z}\} \end{Bmatrix} \quad (3)$$

Further, due to the consideration of orthotropic material in present study, the strain vector, $\{\epsilon\}$ can be decoupled into in-plane strain vector, $\epsilon_b = \{\epsilon_{xx}, \epsilon_{yy}, \gamma_{xy}\}$, and transverse vector, $\epsilon_s = \{\gamma_{yz}, \gamma_{xz}\}$ as

$$\{\epsilon\} = \begin{Bmatrix} \epsilon_b \\ \epsilon_s \end{Bmatrix} = \begin{Bmatrix} \epsilon_{bl} \\ \epsilon_{sl} \end{Bmatrix} + \begin{Bmatrix} \epsilon_{bnl} \\ \epsilon_{snl} \end{Bmatrix} \quad (4)$$

where,

$$\begin{Bmatrix} \epsilon_{bl} \\ \epsilon_{sl} \end{Bmatrix} = \begin{Bmatrix} \mathbf{Z}_{bl}\hat{\epsilon}_{bl} \\ \mathbf{Z}_{sl}\hat{\epsilon}_{sl} \end{Bmatrix} \quad (5)$$

in which,

$$\hat{\epsilon}_{bl} = \begin{Bmatrix} \frac{\partial u_0}{\partial x} \\ \frac{\partial v_0}{\partial y} \\ \frac{\partial u_0}{\partial y} + \frac{\partial v_0}{\partial x} \\ \frac{\partial \phi_x}{\partial x} \\ \frac{\partial \phi_y}{\partial y} \\ \frac{\partial \phi_x}{\partial y} + \frac{\partial \phi_y}{\partial x} \\ \frac{\partial \theta_x}{\partial x} \\ \frac{\partial \theta_y}{\partial y} \\ \frac{\partial \theta_x}{\partial y} + \frac{\partial \theta_y}{\partial x} \end{Bmatrix} \quad \text{and } \hat{\epsilon}_{sl} = \begin{Bmatrix} \frac{\partial w_0}{\partial y} + \phi_y \\ \frac{\partial w_0}{\partial x} + \phi_x \\ \theta_y \\ \theta_x \end{Bmatrix} \quad (6)$$

and

$$\mathbf{Z}_{bl} = \begin{bmatrix} 1 & 0 & 0 & z & 0 & 0 & f(z) & 0 & 0 \\ 0 & 1 & 0 & 0 & z & 0 & 0 & f(z) & 0 \\ 0 & 0 & 1 & 0 & 0 & z & 0 & 0 & f(z) \end{bmatrix}, \quad \mathbf{Z}_{sl} = \begin{bmatrix} 1 & 0 & f'(z) & 0 \\ 0 & 1 & 0 & f'(z) \\ 0 & 0 & 1 & 0 \\ 0 & 0 & 0 & f'(z) \end{bmatrix}$$

Similarly, the nonlinear part of the strain vector, $\{\epsilon\}$, can be written as

$$\begin{Bmatrix} \epsilon_{bnl} \\ \epsilon_{snl} \end{Bmatrix} = \frac{1}{2} \begin{Bmatrix} \mathbf{Z}_{bnl}\hat{\epsilon}_{bnl} \\ \mathbf{Z}_{snl}\hat{\epsilon}_{snl} \end{Bmatrix} = \frac{1}{2} \begin{Bmatrix} \mathbf{Z}_{bnl}\mathbf{A}_b\phi_b \\ \mathbf{Z}_{snl}\mathbf{A}_s\phi_s \end{Bmatrix} \quad (7)$$

and its variational can be denoted as

$$\begin{Bmatrix} \delta\epsilon_{bnl} \\ \delta\epsilon_{snl} \end{Bmatrix} = \begin{Bmatrix} \mathbf{Z}_{bnl}\delta\hat{\epsilon}_{bnl} \\ \mathbf{Z}_{snl}\delta\hat{\epsilon}_{snl} \end{Bmatrix} = \begin{Bmatrix} \mathbf{Z}_{bnl}\mathbf{A}_b\delta\phi_b \\ \mathbf{Z}_{snl}\mathbf{A}_s\delta\phi_s \end{Bmatrix} \quad (8)$$

where,

$$\begin{aligned} \mathbf{Z}_{bnl} &= \begin{bmatrix} 1 & 0 & 0 & z & 0 & 0 & f(z) & 0 & 0 & zf(z) & 0 & 0 & z^2 & 0 & 0 & f^2(z) & 0 & 0 \\ 0 & 1 & 0 & 0 & z & 0 & 0 & f(z) & 0 & 0 & zf(z) & 0 & 0 & z^2 & 0 & 0 & f^2(z) & 0 \\ 0 & 0 & 1 & 0 & 0 & z & 0 & 0 & f(z) & 0 & 0 & zf(z) & 0 & 0 & z^2 & 0 & 0 & f^2(z) \end{bmatrix} \\ \mathbf{Z}_{snl} &= \begin{bmatrix} 1 & 0 & z & 0 & f(z) & 0 & f'(z) & 0 & zf'(z) & 0 & f(z)f'(z) & 0 \\ 0 & 1 & 0 & z & 0 & f(z) & 0 & f'(z) & 0 & zf'(z) & 0 & f(z)f'(z) \end{bmatrix} \end{aligned}$$

The expression for $\mathbf{A}_b\phi_b$ and $\mathbf{A}_s\phi_s$ is given in Appendix A.

Further, the constitutive equation for the k^{th} layer in the hygrothermal environment is as follows

$$\{\sigma_m\}^{(k)} = [\bar{Q}]^{(k)}\{\epsilon^{(k)} - \epsilon_{th}^{(k)}\} = \sigma^{(k)} - \sigma_{th}^{(k)} \quad (9)$$

where, $\{\sigma\}$, $\{\sigma_m\}$, $\{\sigma_{th}\}$, $\{\epsilon\}$, $\{\epsilon_{th}\}$, and $[\bar{Q}]$ are total stress vector, mechanical stress, hygrothermal stress, total strain vector, hygrother-

mal strain vector, and the material constants in the global coordinate, respectively. The hygrothermal strain can be elaborated as follows

$$\{\epsilon_{th}\}^{(k)} = [T_{trans}^{(k)}]^T \begin{Bmatrix} \alpha_1 \\ \alpha_2 \\ 0 \\ 0 \\ 0 \end{Bmatrix} \Delta T + [T_{trans}^{(k)}]^T \begin{Bmatrix} \beta_1 \\ \beta_2 \\ 0 \\ 0 \\ 0 \end{Bmatrix} \Delta C \quad (10)$$

where, α_1 and α_2 are the thermal expansion coefficient, and β_1 and β_2 are the moisture coefficients of the k^{th} layer in the local material (1–2–3) coordinate system. The notation, $T_{trans}^{(k)}$, is the coordinate transformation matrix [71]. The change in temperature and moisture with respect to a reference value is given by ΔT and ΔC , respectively. Consequently, the in-plane stress resultants can be found as mentioned in Appendix B.

2.1. Equation of motion

For arbitrary space variable and admissible virtual displacement, $\delta\{u, v, w\}$, Hamilton's principle of the given system using total Lagrangian approach is written as

$$\delta \int_{t_i}^{t_f} \mathcal{L} dt = \int_{t_i}^{t_f} (\delta \mathcal{K} - \delta \mathcal{U} + \delta \mathcal{W}_{\text{ext}}) dt = 0 \quad (11)$$

Kinetic energy. The virtual kinetic energy of the system is expressed as follows

$$\int_{t_i}^{t_f} \delta \mathcal{K} dt = - \int_{t_i}^{t_f} \int_V \rho \delta\{u\}^T \ddot{u} dV dt \quad (12)$$

where, ρ is the mass density of the material; t_i and t_f are the initial and final time of consideration for the analysis, respectively.

Strain energy. The virtual strain energy of a laminated plate due to mechanical strain and the artificial constraints is expressed as,

$$\delta \mathcal{U} = \int_V \delta\{\epsilon\}^T \{\sigma\} dV + \delta \mathcal{U}_\gamma \quad (13)$$

where, $\delta \mathcal{U}_\gamma$ is the virtual strain energy due to artificial constraints with penalty parameter, γ and is expressed as

$$\delta \mathcal{U}_\gamma = \gamma \int_V \left\{ \delta \left(\phi_x + \frac{\partial w_0}{\partial x} \right)^T \left(\phi_x + \frac{\partial w_0}{\partial x} \right) + \delta \left(\phi_y + \frac{\partial w_0}{\partial y} \right)^T \left(\phi_y + \frac{\partial w_0}{\partial y} \right) \right\} dV \quad (14)$$

Work done by external forces. The virtual work done due to transverse mechanical loading, $P(x, y, t)$ is written as

$$\delta \mathcal{W}_{\text{ext}} = \int_A \delta w^T P dA \quad (15)$$

2.2. Finite element formulation

For finite element discretization, a nine-noded isoparametric element with seven degrees of freedom (DOFs) per node is considered. The present finite element utilizes the same Lagrange basis function for both generalization of field variables and geometry; and described as

$$\{u\} = \sum_{i=1}^9 N_i q_i, \quad x = \sum_{i=1}^9 N_i x_i, \quad y = \sum_{i=1}^9 N_i y_i \quad (16)$$

where, $\{u\} = (u_0, v_0, w_0, \phi_x, \phi_y, \theta_x, \theta_y)^T$ is the generalized field variables; q_i is the corresponding nodal field variables associated with i^{th} node; and (x, y) are the generalized geometric coordinate, in which x_i and y_i are the geometric coordinate values of the corresponding i^{th} node.

Using the expression of displacement vector, $\{u\}$ from Eq. (16), the generalized linear bending strain vector, \hat{e}_{bl} and the generalized linear shear strain vector, \hat{e}_{sl} at any point can be written as

$$\hat{e}_{bl} = \mathbf{B}_{bl} \mathbf{q} = \sum_{i=1}^9 \mathbf{B}_{bli} \mathbf{q}_i \hat{e}_{sl} = \mathbf{B}_{sl} \mathbf{q} = \sum_{i=1}^9 \mathbf{B}_{sli} \mathbf{q}_i \quad (17)$$

where,

$$\{\mathbf{q}\} = \{q_1^T \quad q_2^T \quad \dots \quad q_8^T \quad q_9^T\}^T \quad \mathbf{q}_i = \{u_{0i} \quad v_{0i} \quad w_{0i} \quad \phi_{xi} \quad \phi_{yi} \quad \theta_{xi} \quad \theta_{yi}\}^T$$

Similarly, for the nonlinear terms

$$\begin{aligned} \hat{e}_{bnl} &= \mathbf{B}_{bnl} \mathbf{q} = \sum_{i=1}^9 \mathbf{B}_{bnli} \mathbf{q}_i = \sum_{i=1}^9 \mathbf{A}_b \mathbf{G}_{bnli} \mathbf{q}_i \\ \hat{e}_{snl} &= \mathbf{B}_{snl} \mathbf{q} = \sum_{i=1}^9 \mathbf{B}_{snli} \mathbf{q}_i = \sum_{i=1}^9 \mathbf{A}_s \mathbf{G}_{snli} \mathbf{q}_i \end{aligned} \quad (18)$$

and the \mathbf{B}_{bli} , \mathbf{B}_{sli} , \mathbf{G}_{bnli} , and \mathbf{G}_{snli} are presented in Appendix C

Stiffness matrix. The elemental stiffness matrix of the plate element is given by

$$\mathbf{K} = \mathbf{K}_I + \mathbf{K}_\gamma + \mathbf{K}_g \quad (19)$$

where

$$\mathbf{K}_I = \int_A (\mathbf{B}_{bl}^T \mathbf{D}_{bl} \mathbf{B}_{bl} + \mathbf{B}_{sl}^T \mathbf{D}_{sl} \mathbf{B}_{sl}) dA$$

in which

$$\mathbf{D}_{lbl} = \int_{-\frac{h}{2}}^{\frac{h}{2}} \mathbf{Z}_{bl}^T \bar{Q}_b \mathbf{Z}_{bl} dz, \quad \mathbf{D}_{lsl} = \int_{-\frac{h}{2}}^{\frac{h}{2}} \mathbf{Z}_{sl}^T \bar{Q}_s \mathbf{Z}_{sl} dz,$$

and the expression for penalty stiffness matrix, \mathbf{K}_γ is

$$\mathbf{K}_\gamma = \int_A \gamma \mathbf{B}_\gamma^T \mathbf{B}_\gamma h dA$$

where

$$\mathbf{B}_\gamma \mathbf{q} = \mathbf{B}_{\gamma i} \mathbf{q}_i$$

in which

$$\mathbf{B}_{\gamma i} = \begin{bmatrix} 0 & 0 & \frac{\partial N_i}{\partial y} & N_i & 0 & 0 & 0 \\ 0 & 0 & \frac{\partial N_i}{\partial x} & 0 & N_i & 0 & 0 \end{bmatrix}$$

It is important to have a proper value of the penalty parameter to avoid the ill-conditioning of the stiffness matrix, \mathbf{K} comprised of mechanical strain and strain energy due to penalty, and hence ensure the accuracy of the analysis. It is often customary to take the penalty as large as possibly compatible with the computer hardware architecture for software implementation. Nevertheless, the penalty parameter of the order of transverse elastic modulus, E_2 is considered in this present work.

Further, \mathbf{K}_g is the initial stiffness matrix due to initial stresses at particular time, and the expression for \mathbf{K}_g is given by

$$\mathbf{K}_g = \int_A (\mathbf{G}_{bnli}^T \mathbf{S}_b \mathbf{G}_{bnli} + \mathbf{G}_{snli}^T \mathbf{S}_s \mathbf{G}_{snli}) dA \quad (20)$$

in which \mathbf{S}_b and \mathbf{S}_s are given in Appendix D.

To carry out the dynamic analysis under the hygrothermal environment, the static deflection due to thermal and moisture is first evaluated by using the equilibrium equation (Eq. (21)).

$$(\mathbf{K}_I + \mathbf{K}_\gamma) \mathbf{q}'' = \mathbf{F}_{\Delta T} \quad (21)$$

Then utilizing the static deflection, \mathbf{q}'' , the geometric stiffness matrix, \mathbf{K}_g is evaluated by considering Green–Lagrange strain–displacement relation.

Mass matrix.

$$\mathbf{M} = \int_A \mathbf{R}^T \mathbf{m} \mathbf{R} dA \quad (22)$$

where

$$\mathbf{m} = \int_{-h/2}^{h/2} \rho \begin{bmatrix} 1 & 0 & 0 & z & 0 & f(z) & 0 \\ 0 & 1 & 0 & 0 & z & 0 & f(z) \\ 0 & 0 & 1 & 0 & 0 & 0 & 0 \\ z & 0 & 0 & z^2 & 0 & zf(z) & 0 \\ 0 & z & 0 & 0 & z^2 & 0 & zf(z) \\ f(z) & 0 & 0 & zf(z) & 0 & f(z)^2 & 0 \\ 0 & f(z) & 0 & 0 & zf(z) & 0 & f(z)^2 \end{bmatrix} dz$$

and

$$\mathbb{R}\mathbf{q} = \sum_{i=1}^9 N_i I_7 \mathbf{q}_i$$

in which I_7 is the identity matrix of order seven.

Elemental load vector.

$$\mathbf{F}_m = \int W^T P dA \quad (23)$$

where

$$W = \{W_1 \ W_2 \ W_3 \ W_4 \ W_5 \ W_6 \ W_7 \ W_8 \ W_9\}$$

in which

$$W_i = [0 \ 0 \ N_i \ 0 \ 0 \ 0 \ 0]$$

Governing equation. To obtain the governing equations, Eqs. (12), (13) and (15), are substituted in Eq. (11), and then finite element discretization is employed using Eq. (16). After eliminating the virtual displacement, δq , the system of equations of motion can be obtained in the following matrix form.

$$M\ddot{\mathbf{q}} + K\mathbf{q} = \mathbf{F}_m \quad (24)$$

The governing set of equations for eigenvalue characterization of the system is obtained as

$$M\ddot{\mathbf{q}} + K\mathbf{q} = 0 \quad (25)$$

2.3. Folded plate formulation

For the finite element formulation of the folded plate, the schematic geometries, shown in Fig. 2, are considered. In the above section, the governing equation pertaining to dynamic analysis of laminated composite flat plate under hygrothermal environment is shown, now the elemental matrices are modified by a transformation matrix as presented in Eq. (26) to accommodate the folding in the plate structure. Therefore, two drilling degrees of freedom, ϕ_z and θ_z are considered to expand the seven degrees of freedom (i.e.,

$u_0, v_0, w_0, \phi_x, \phi_y, \theta_x, \theta_y$) into nine degrees of freedom (i.e., $u_0, v_0, w_0, \phi_x, \phi_y, \phi_z, \theta_x, \theta_y, \theta_z$). The elemental matrices corresponding to the drilling degrees of freedom are populated with a very small value which is a thousand times smaller than the smallest diagonal values [67]. The transformation matrix is operated on the elemental stiffness matrix, mass matrix, and force vector to get the respective matrices and vector in the global coordinate system of the folded plate as follows.

$$\left\{ \begin{array}{l} u_0 \\ v_0 \\ w_0 \\ \phi_x \\ \phi_y \\ \phi_z \\ \theta_x \\ \theta_y \\ \theta_z \end{array} \right\} = \left[\begin{array}{ccccccc} C(x, X) & C(x, Y) & C(x, Z) & 0 & 0 & 0 & 0 \\ C(y, X) & C(y, Y) & C(y, Z) & 0 & 0 & 0 & 0 \\ C(z, X) & C(z, Y) & C(z, Z) & 0 & 0 & 0 & 0 \\ 0 & 0 & 0 & C(y, Y) & -C(y, X) & C(y, Z) & 0 \\ 0 & 0 & 0 & -C(x, Y) & C(x, X) & -C(x, Z) & 0 \\ 0 & 0 & 0 & C(z, Y) & -C(z, X) & C(z, Z) & 0 \\ 0 & 0 & 0 & 0 & 0 & 0 & C(y, Y) \\ 0 & 0 & 0 & 0 & 0 & 0 & -C(y, X) \\ 0 & 0 & 0 & 0 & 0 & 0 & C(x, X) \\ 0 & 0 & 0 & 0 & 0 & 0 & -C(x, Z) \\ 0 & 0 & 0 & 0 & 0 & 0 & C(z, Y) \\ 0 & 0 & 0 & 0 & 0 & 0 & -C(z, X) \\ 0 & 0 & 0 & 0 & 0 & 0 & C(z, Z) \end{array} \right] \left\{ \begin{array}{l} u'_0 \\ v'_0 \\ w'_0 \\ \phi'_x \\ \phi'_y \\ \phi'_z \\ \theta'_x \\ \theta'_y \\ \theta'_z \end{array} \right\} \quad (26)$$

where, x and X represent the local and global coordinate system, respectively. The field variables with prime notation denote the global coordinate field variable. The notation $C(x, X)$ represents the cosine of the angle between local and global coordinate positions.

In brief, the above equation can be written as

$$\{\mathbf{u}\} = [\mathbf{T}]\{\mathbf{u}'\} \quad (27)$$

Following the transformation as mentioned in Ref. [67], the governing equations for the free and forced vibration problem can be stated as follows.

$$[\bar{M}]\ddot{\mathbf{q}}' + [\bar{K}]\mathbf{q}' = 0 \quad (28)$$

and

$$[\bar{M}]\ddot{\mathbf{q}}' + [\bar{K}]\mathbf{q}' = \bar{\mathbf{F}}_m(t) \quad (29)$$

where $\ddot{\mathbf{q}}'$ and \mathbf{q}' are the acceleration and displacement vector of the folded plate. $\bar{\mathbf{F}}_m(t)$ is the transverse load applied at the surface of the plate.

Rayleigh damping. Although damping properties are inherently found in the mechanical system, modeling the exact damping characteristic is a difficult task. Damping ratios for various modes are actually obtained by the experimental approach. And the obtained damping ratio is used to model the damping by Rayleigh damping model, which is a special case of the Caughey series [72].

Rayleigh damping is modeled as a linear combination of the mass and stiffness matrices, that is,

$$\bar{C} = \alpha \bar{M} + \beta \bar{K} \quad (30)$$

where, α and β are Rayleigh damping coefficients, which are obtained for a particular frequency bandwidth by Eq. (31).

$$\xi_n = \frac{\alpha}{2} \frac{1}{\omega_n} + \frac{\beta}{2} \omega_n \quad (31)$$

where, ξ_n is the damping ratio and ω_n is the natural frequency of n^{th} mode. For two selected i^{th} and j^{th} mode, α and β can be obtained as

$$\left\{ \begin{array}{l} \alpha \\ \beta \end{array} \right\} = \left[\begin{array}{cc} \frac{1}{2\omega_i} & \frac{\omega_i}{2} \\ \frac{1}{2\omega_j} & \frac{\omega_j}{2} \end{array} \right]^{-1} \left\{ \begin{array}{l} \xi_i \\ \xi_j \end{array} \right\} \quad (32)$$

Thus, after consideration of damping, the equation of motion becomes

$$\bar{M}\ddot{\mathbf{q}}' + \bar{C}\dot{\mathbf{q}}' + \bar{K}\mathbf{q}' = \bar{\mathbf{F}}_m \quad (33)$$

3. Results and discussions

In this section, detailed analysis and discussion of the dynamic behavior of laminated composite flat and folded plate are presented under the hygrothermal environment. The above-shown formulation

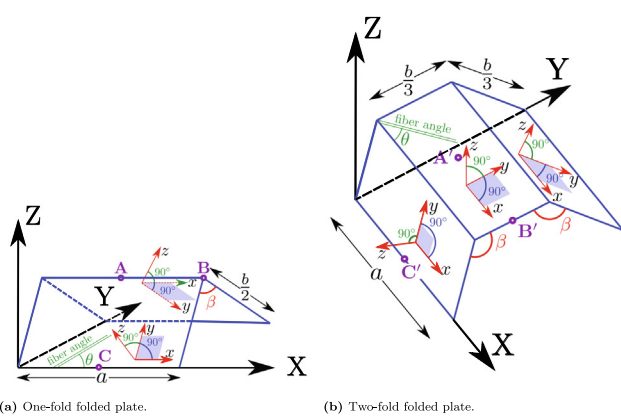


Fig. 2. Schematic diagram of onefold and twofold folded plate with fold angle β .

Table 1

Elastic moduli of graphite-epoxy lamina at different temperatures, $\alpha_1 = -0.3 \times 10^{-6}/K$, $\alpha_2 = 28.1 \times 10^{-6}/K$.

Elastic moduli (GPa)	Temperature (K)					
	300	325	350	375	400	425
E_1	172.5	172.5	172.5	172.5	172.5	172.5
E_2	6.9	6.17	5.81	5.45	5.08	4.9
G_{12}	3.45	3.45	3.16	2.88	2.73	2.59

Table 2

Elastic moduli of graphite/epoxy lamina at different moisture concentration, $\beta = 0$, $\beta = 0.44$

Elastic Moduli (GPa)	Moisture concentration, C(%)						
	0	0.25	0.5	0.75	1.00	1.25	1.50
E_1	172.5	172.5	172.5	172.5	172.5	172.5	172.5
E_2	6.9	6.72	6.54	6.36	6.17	6.17	6.17
G_{12}	3.45	3.45	3.45	3.45	3.45	3.45	3.45

Table 3

Properties of Graphite-epoxy composite at different temperatures ($\alpha_1 = -0.3 \times 10^{-6}/K$, $\alpha_2 = 28.1 \times 10^{-6}/K$)

Elastic constants (GPa)	Temperature (K)					
	300 K	325 K	350 K	375 K	400 K	425 K
E_1	130.0	130.0	130.0	130.0	130.0	130.0
E_2	9.5	8.5	8.0	7.5	7.0	6.75
$G_{12} = G_{13}$	6.0	6.0	5.5	5.0	4.75	4.5

Table 4

Properties of graphite-epoxy composites at different moisture concentration ($\beta_1 = 0$, $\beta_2 = 0.44$)

Elastic constants (GPa)	Moisture concentration (%)						
	0.0	0.25	0.50	0.75	1.00	1.25	1.50
E_1	130.0	130.0	130.0	130.0	130.0	130.0	130.0
E_2	9.5	9.25	9.0	8.75	8.5	8.5	8.5
$G_{12} = G_{13}$	6.0	6.0	6.0	6.0	6.0	6.0	6.0

is used for the generalized development of finite element computer code using MATLAB, which investigates free vibration natural frequencies, transient displacement and stresses, and harmonic analysis. The Newmark's scheme with $\alpha = 0.5$ and $\beta = 0.25$ is used for the transient analysis. The penalty approach is considered for the incorporation of C^0 Lagrange element. The effect of the penalty parameter for both flat and folded plates is found to be the same, hence, it is kept equal for both cases as $\gamma = 10^{10}$. In the first part, free vibration analysis has been carried out to evaluate natural frequency. In the second part, transient analysis under the hygrothermal environment is performed. In the third and last part of the section, the steady-state response for mechanical-thermal load has been investigated. The mesh size of (8×8) has been considered for flat plate and onefold folded plate, whereas (6×9) has been taken for the twofold folded plate. Further, (3×3) Gauss-integration point for the bending and (2×2) Gauss-integration point for the shear part have been employed for the numerical integration.

3.1. Material properties

The following sets of material properties are used for the present analysis. Some materials are hygrothermal dependent, so the variation of the properties with the temperature and moisture are also given.

- MM1 [18]: $G_{12} = 0.6E_2$, $G_{23} = 0.5E_2$, $\nu_{12} = \nu_{13} = \nu_{23} = 0.25$, $E_3 = E_2$
- MM2 [49]: $E_1 = 60.7 \times 10^9 N/m^2$, $E_2 = 24.8 \times 10^9 N/m^2$, $G_{12} = G_{13} = G_{23} = 12.0 \times 10^9 N/m^2$, $\nu_{12} = \nu_{21} = 0.23$, $\rho = 1300 kg/m^3$
- MM3 [15]: $G_{13} = G_{12}$, $G_{23} = 0.4G_{12}$, $\nu_{12} = 0.25$, $\rho = 1600 kg/m^3$ other properties are mentioned in Tables 1 and 2.
- MM4 [42]: $E_1 = 25E_2$, $E_2 = 2.1 \times 10^6 N/cm^2$, $G_{12} = G_{13} = 0.5E_2$, $G_{23} = 0.2E_2$, $\nu_{12} = 0.25$, $\rho = 8 \times 10^{-6} N.s^2/cm^4$
- MM5 [68]: $G_{23} = G_{12}$, $G_{23} = 0.5G_{12}$, $\rho = 1600 kg/m^3$, $\nu_{12} = 0.3$ other properties are mentioned in Tables 3 and 4.

3.2. Various types of loading

The analysis of laminated composite plates is considered under the application of various time-dependent blast pulse loads. And these loads are defined and expressed as follows:

- Step loading

$$F(t) = \begin{cases} 1, & 0 \leq t \leq t_1 \\ 0 & t \geq t_1 \end{cases}$$

Where t_1 is the positive phase duration of load.

- Sinusoidal loading

$$F(t) = \begin{cases} \sin(\pi t/t_1), & 0 \leq t_1 \\ 0, & t \geq t_1 \end{cases}$$

- Explosive blast loading

$$F(t) = \begin{cases} e^{-\gamma t}, & 0 \leq t \leq t_1 \\ 0, & t \geq t_1 \end{cases}$$

where, γ denotes a decay parameter. The value of $\gamma = 660 s^{-1}$ has been considered.

- Triangular loading

$$F(t) = \begin{cases} 1 - t/t_1, & 0 \leq t \leq t_1 \\ 0, & t \leq 0, \text{ and } t \geq t_1 \end{cases}$$

- The spatial pressure applied for the analysis are defined by

$$P(x, y, t) = \begin{cases} P_0 \sin(\pi x/a) \sin(\pi y/b) F(t), & \text{Sinusoidal distributed loading} \\ P_0 F(t), & \text{Uniformly distributed loading} \end{cases}$$

3.3. Boundary conditions

As the present formulation is based on the displacement approach, so it is required to satisfy the kinematics boundary conditions ($u'_0, v'_0, w'_0, \phi'_x, \phi'_y, \phi'_z, \theta'_x, \theta'_y, \theta'_z$) only. The different types of boundary conditions, most commonly occurring in practice are considered for finite element analysis of laminated composite flat and folded plates to assess the efficacy of the present approach.

- Simply Supported

1. SSSS-1:

$$v'_0 = w'_0 = \phi'_y = \phi'_z = \theta'_y = \theta'_z = 0 \text{ at } x = 0, a; \\ u'_0 = w'_0 = \phi'_x = \phi'_z = \theta'_x = \theta'_z = 0 \text{ at } y = 0, b.$$

2. SSSS-2:

$$u'_0 = w'_0 = \phi'_x = \phi'_z = \theta'_y = \theta'_z = 0 \text{ at } x = 0, a; \\ v'_0 = w'_0 = \phi'_y = \theta'_x = \theta'_z = 0 \text{ at } y = 0, b.$$

- Clamped boundary condition

$$\text{CCCC: } u'_0 = v'_0 = w'_0 = \phi'_x = \phi'_y = \phi'_z = \theta'_x = \theta'_y = \theta'_z = 0 \text{ at } x = 0, a \text{ and } y = 0, b.$$

- An arbitrary boundary condition

ABCD: 'A' at $y = 0$, 'B' at $y = b$, 'C' at $x = a$, and 'D' at $x = 0$; where A, B, C, and D can be any boundary condition.

3.4. Free vibration analysis

The natural frequency of the structure is an important parameter to design a structure and safeguard it from failure due to resonance, etc.

Table 5

Convergence study of present finite element solution for symmetric and anti-symmetric laminates

Lamination Scheme	a/h	$\bar{\omega} = \omega a^2/h\sqrt{\rho/E_2}$				
		2×2	4×4	6×6	8×8	10×10
[0°/90°/90°/0°]	10	15.282	15.182	15.176	15.175	15.175
[0°/90°/90°/0°]	20	17.849	17.69	17.681	17.679	17.679
[0°/90°/0°/90°]	10	14.957	14.846	14.839	14.838	14.838
[0°/90°/0°/90°]	20	16.738	16.581	16.572	16.570	16.570

Due to the detrimental effect of change in temperature and moisture of the operating environment, free vibration analysis of laminated composite plate under the hydrothermal environment is an essential requirement. Therefore, the effect of various parameters on the natural frequencies is extensively evaluated to get a better understanding of the free vibration behavior of flat and folded laminated composite plates under thermal and moisture variation. A subspace iteration technique is utilized for the free vibration analysis [73].

3.4.1. Cross-ply laminated composite plate without any hydrothermal load

To assess the efficacy of present formulation, a convergence study has been performed for the free vibration analysis. To obtain the converge frequency, a simply supported (SSSS1) cross-ply symmetric and anti-symmetric laminated composite plate having side-to-thickness ratio ($a/h = 10, 20$) is considered. The considered composite plate is made up of material having properties like $E_1/E_2 = 40, G_{12} = G_{13} = 0.6E_2, G_{23} = 0.5E_2, \nu_{12} = 0.25$, and $\rho = 1$ [74]. The obtained non-dimensional frequencies ($\bar{\omega} = \omega a^2/h\sqrt{\rho/E_2}$) for different number of elements are shown in Table 5. The solution is found to be converging at element size 8×8 .

Further, to validate the present formulation, the cross-ply laminated composite plates with various types of lamination schemes are considered for the free vibration analysis without any hydrothermal load. The plate with side-to-thickness ratio ($a/h = 5$), made of material MM1, is under simply supported (SSSS-1) boundary condition. The non-dimensional natural frequencies, $\bar{\omega} = 10\omega h\sqrt{\rho/E_2}$, are calculated for various E_1/E_2 ratios. The obtained solutions are shown in Table 6 and are found to be in good agreement with the available solutions in the literature. The formulation is validated for different layers of a cross-ply laminated composite plate with varying E_1/E_2 ratio. As the number of layers increases, the non-dimensional frequency also increases due to an increase in the stiffness of the structure. Moreover, the non-dimensional frequency is also found to be increasing with an increase in modulus ratio E_1/E_2 due to higher fiber-direction elasticity modulus contribution.

3.4.2. Effect of change in temperature and moisture on anti-symmetric square laminated plate

An anti-symmetric cross-ply [0°/90°]2 and angle-ply [45°/−45°]2 laminated composite plates are considered to assess the effect of thermal and moisture loads on the free vibration characteristics. The plate has dimensions, $a = b = 0.5 m$, with thickness, $h = 5 mm$, and made of material MM3. The simply supported SSSS-1 and SSSS-2 boundary conditions are considered for cross-ply and angle-ply laminated composite plates, respectively. The thermal and moisture loads are applied by a uniform change in temperature, $\Delta T = T - 300 = \text{constant}$, and moisture, $\Delta C = C = \text{Constant}$, respectively. The temperature, $T = 300 K$, and the moisture, $C = 0\%$, are references assumed for the analysis. The obtained results are shown in Figs. 7 and 8 and are found to be in good agreement with the available solution. Due to the depreciable nature of the hydrothermal strain to the total strain, the increase in temperature and moisture reduces the natural frequency. It is observed in Table 7 that almost 41% increase in temperature caused 4.2% decrease in the natural frequency for four-layered

Table 6Non-dimensional fundamental frequencies of simply supported cross-ply square laminated plate with $a/h = 5$ and material MM1 under SSSS1 boundary condition

No. of layers	Source	E_1/E_2				
		3	10	20	30	40
$[0^0/90^0]$	Present	2.4868	2.7946	3.1246	3.3941	3.6221
	Patel et al. [18]	2.4935	2.7886	3.0778	3.2940	3.4638
	Noor (3D Elastic) [75]	2.5031	2.7938	3.0698	3.2705	3.4250
$[0^0/90^0]_2$	Present	2.6004	3.2782	3.8505	4.2138	4.4685
	Patel et al. [18]	2.6029	3.2488	3.7677	4.0841	4.3001
	Noor (3D Elastic) [75]	2.6182	3.2578	3.7622	4.0660	4.2719
$[0^0/90^0]_3$	Present	2.6224	3.3622	3.9673	4.3420	4.6005
	Patel et al. [18]	2.6264	3.3478	3.9219	4.2686	4.5035
	Noor (3D Elastic) [75]	2.6440	3.3657	3.9359	4.2783	4.5091
$[0^0/90^0]_5$	Present	2.6338	3.4051	4.0270	4.4077	4.6688
	Patel et al. [18]	2.6390	3.4018	4.0093	4.3770	4.6279
	Noor (3D Elastic) [75]	2.6583	3.4250	4.0337	4.4011	4.6498

Table 7Natural frequencies (Hz) of square laminated plate with $a/h = 100$ at elevated temperature, T

Lamination Scheme	Source/Method	Temperature T(K)					
		300	325	350	375	400	425
$[0^0/90^0]_2$	Present	92.704	91.676	90.698	89.887	89.293	88.82
	Parhi et al. [15]	92.72	92.47	92.26	92.09	91.96	92.82
	Huang et al. [76]	92.70	92.23	91.43	90.85	90.56	90.25
$[45^0/-45^0]_2$	Present	124.23	112.87	102.44	92.958	84.902	75.433
	Parhi et al. [15]	124.26	113.42	103.36	94.32	86.77	77.76
	Huang et al. [76]	124.23	112.89	102.46	92.97	84.85	75.46

Table 8Natural frequency (Hz) of square laminated plate at elevated moisture concentration, C with $a/h = 100$

Lamination scheme	Source/Method	Moisture concentration (%)					
		0	0.25	0.5	0.75	1	1.5
$[0^0/90^0]_2$	Present	92.704	91.205	89.753	88.351	87.003	84.223
	Parhi et al. [15]	92.72	92.16	91.63	91.13	90.65	89.60
	Huang et al. [76]	92.70	92.10	92.58	90.98	90.46	89.42
$[45^0/-45^0]_2$	Present	124.23	98.058	64.096	-	-	-
	Parhi et al. [15]	124.26	98.23	64.58	-	-	-
	Huang et al. [76]	124.23	98.27	64.26	-	-	-

cross-ply $[0^0/90^0]_2$ plate, whereas, the same elevation of temperature caused 39.27% decrease in the natural frequency of four-layered angle-ply $[45^0/-45^0]_2$ laminated plate. Further, the effect of moisture on the cross-ply and angle-ply is also found to be very contrasting, as the 0.5% increase in moisture reduced the natural frequency by almost 3.2% for cross-ply, whereas 48.4% for the angle-ply laminate as shown in Table 8. In other words, it is observed that the angle-ply laminated plate shows a larger rate of reduction in the natural frequency with an increase in temperature and moisture than the cross-ply laminated plate. This variation between cross-ply and angle-ply is due to the fact that the several elemental entries of ABD-matrix of anti-symmetric cross-ply become zero, such as $B_{26} = B_{16} = 0$ and $C_{12} = C_{16} = C_{26} = 0$ in contrast to the anti-symmetric angle-ply where these terms are nonzero and add up to increase the stiffness of the angle-ply. So, angle-ply seems to be more susceptible to the hygrothermal load than the cross-ply. Hence, it can be argued that the use of cross-ply laminate is more beneficial in the context of a hygrothermal environment; nevertheless, it is subjective to many other parameters too.

3.4.3. Effect of various parameters on the natural frequency of laminated composite plate under hygrothermal environment

In this section, the variation of natural frequency for various parameters such as side-to-thickness ratio, number of layers, and fiber orientation are assessed under the temperature and moisture concentration variation. The plate used for the analysis have dimensions as $a = b = 0.5\text{ m}$, and $h = 5\text{ mm}$, with material property MM3. Again the boundary conditions SSSS-1 and SSSS-2 are considered for cross-ply and angle-ply, respectively. The thermal and moisture concentration are varied uniformly as $\Delta T = T - 300 = \text{constant}$, and $\Delta C = C = \text{constant}$. The obtained natural frequencies are plotted against various parameters and shown in Fig. 3. The Fig. 3a and Fig. 3b show the variations of natural frequencies against change in temperature for $a/h = 100$ and $a/h = 10$, respectively. It is observed in Fig. 3a that the frequency variation of three-layered $[0^0/90^0/0^0]$ and four-layered $[0^0/90^0/90^0/0^0]$ symmetric laminate is almost the same, while four-layered $[0^0/90^0/0^0/90^0]$ anti-symmetric laminate shows a lot of difference in the natural frequency due to twisting tendency found in the anti-symmetric laminate caused by the thermal

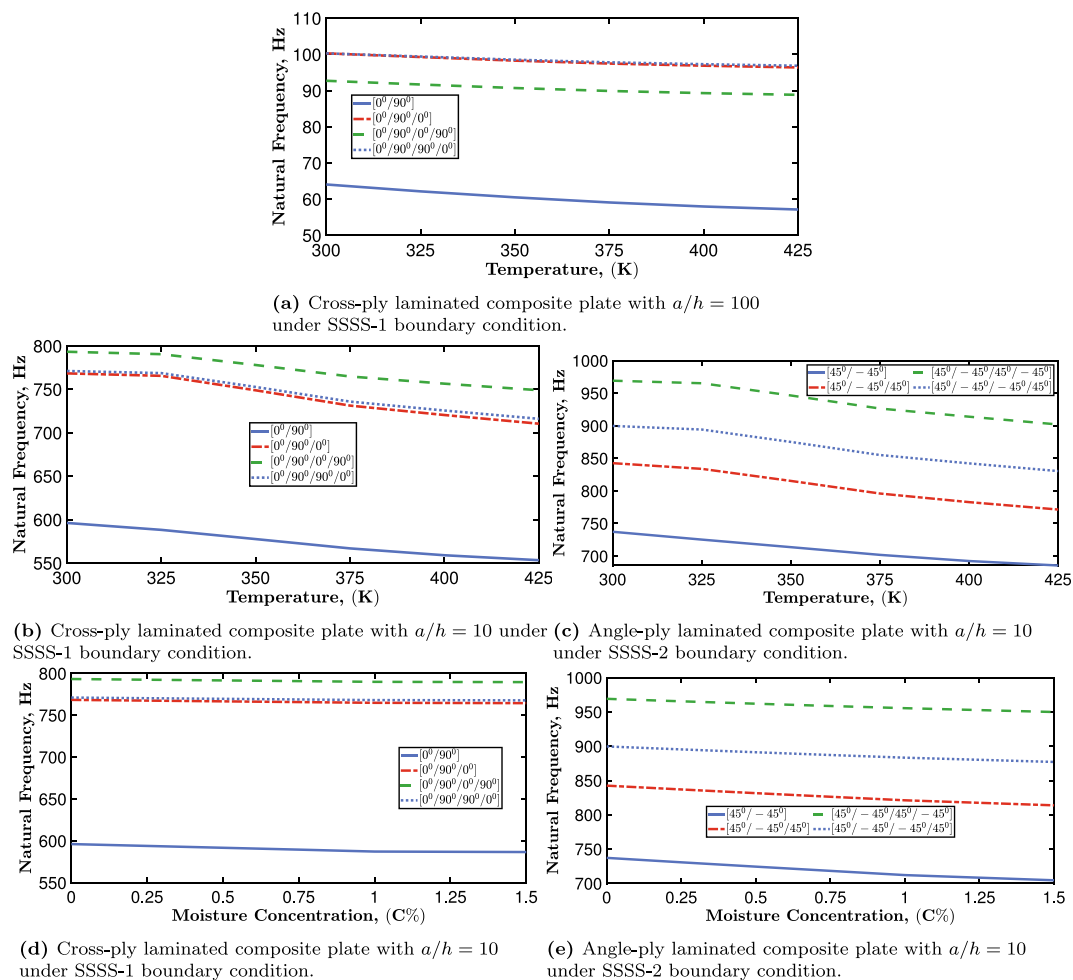


Fig. 3. variation of natural frequency (Hz) of laminated composite plate for different temperature and moisture concentration under various parameters.

load. Moreover, Fig. 3b shows that unlike the solution for $a/h = 100$, the solution of $a/h = 10$ has a higher frequency for anti-symmetric $[0^\circ/90^\circ/0^\circ/90^\circ]$ laminate as the coupling between bending and extension is highly dependent on the thickness, which increases the stiffness of the anti-symmetric cross-ply in contrast to the symmetric cross-ply laminate. Also, for $a/h = 10$, the difference in natural frequency of $[0^\circ/90^\circ/0^\circ]$ and $[0^\circ/90^\circ/90^\circ/0^\circ]$ are not much due to the symmetric nature of the laminate. Further, Fig. 3c shows the frequency variation with a change in temperature for angle-ply laminate. Moreover, unlike the cross-ply laminate, the variations of frequencies for all the four angle-ply lamination schemes are different. The same pattern is found

in Figs. 3d and 3e for the change in moisture concentration with respect to cross-ply and angle-ply laminate under thermal load. Overall, it can be said that the hydrothermal environment adversely affects the laminate, and it profoundly depends on the lamination schemes as well.

Moreover, the natural frequency variations with side-to-thickness ratio and fiber orientation under thermal load have also been evaluated and shown in Fig. 4. It is observed in Fig. 4a that as side-to-thickness ratio (a/h) increases, the natural frequency decreases due to stiffness being directly dependent on the thickness. However, the variation of frequency among the symmetric cross-ply and angle-ply

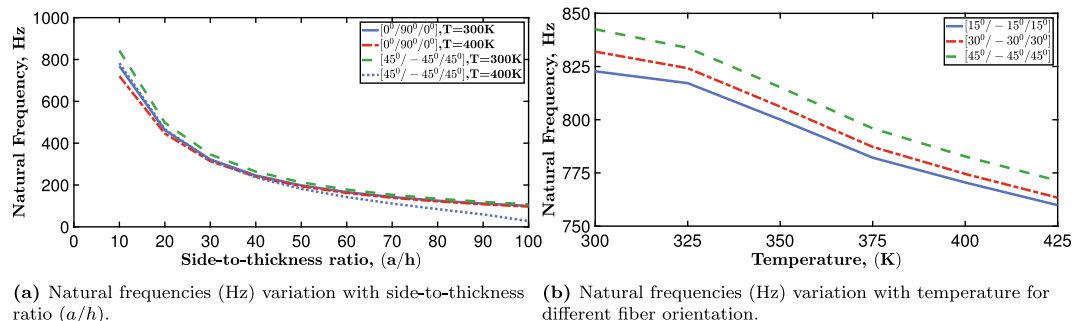


Fig. 4. Variation of natural frequency (Hz) of laminated composite plate having $a/h = 10$ under thermal load.

is not much. Further, the Fig. 4b shows the variation of frequency for varying angles of three-layered symmetric angle-ply. It is observed that the natural frequency increases with an increase in ply-angle due to an increase in stiffness with an increase in angle; however, it decreases with an increase in temperature due to a decrease in stiffness with an increase in temperature.

3.4.4. Natural frequency of one-fold folded laminated composite plate under hygrothermal environment

In this section, one-fold folded laminated composite plates (as shown in Fig. 2a) having various lamination schemes with different thicknesses are considered for the free vibration analysis under the hygrothermal environment. The plate has sides-length as $a = b = 1.5 \text{ m}$, and different thicknesses as $h = 7 \text{ mm}, 9 \text{ mm}, 15 \text{ mm}$. The plate is made up of hygrothermal-dependent material properties MM5. The natural frequencies of anti-symmetric $[0^\circ/90^\circ]_2$ and symmetric $[0^\circ/90^\circ]_s$ laminated composite plates for the crank angle $\beta = 90^\circ, 120^\circ, 180^\circ$ are evaluated for various temperatures. The obtained frequencies for clamped (CCCC) boundary condition are shown in Tables 9 and 10. Due to the utilization of higher-order non-polynomial shear deformation theory, the present obtained solutions are found to be better than the available solution of Das and Niyogi [68]. As the FSDT solutions presented by Das and Niyogi [68] over-predict the natural frequency. Further, a significant discrepancy is found in the natural frequency of folded plate and flat plate, because fold in the plate increases the stiffness of the plate due to participation of in-plane stiffness into bending stiffness. Moreover, the change in natural frequencies with respect to temperature is greater in the folded

plate than in the flat plate. This observation emphasizes the need for the folded plate analysis under the hygrothermal environment. The natural frequency of the folded plate is also found to be varying a lot with the change in moisture concentration. And the discrepancies between flat and folded results are found to be significant due to the combined effect of folding and the hygrothermal effect. Further, the blank space in Tables 9 and 10 denotes the instability state.

After the validation of the result for the one-fold folded laminated composite plate. The pattern of variation of natural frequency with respect to the temperature and moisture for cross-ply and angle-ply laminate is evaluated and shown in Fig. 5. In this case the side-to-thickness ratio, $a/h = 10$ has been considered. Fig. 5 reveals that the effect of folding on the natural frequencies for the angle-ply is less than the cross-ply as the pattern shown in Figs. 5a and 5b are the same, however, the frequency pattern for the cross-ply is a little different. The same pattern is observed for the moisture concentration variation shown in Figs. 5c and 5d.

3.4.5. Natural frequency of two-fold folded laminated composite plate under hygrothermal environment

In this section, two-fold folded laminated composite plates (as shown in Fig. 2b) having various lamination schemes with different thicknesses are considered for the free vibration analysis under the hygrothermal environment. The plate dimensions are: $a = 1.5 \text{ m}$, $b = 2.25 \text{ m}$, and thickness, $h = 7 \text{ mm}, 9 \text{ mm}, 15 \text{ mm}$. The plate is made up of hygrothermal-dependent material properties MM5. The natural frequencies with varying temperature and moisture for clamped (CCCC) boundary condition are obtained and presented in

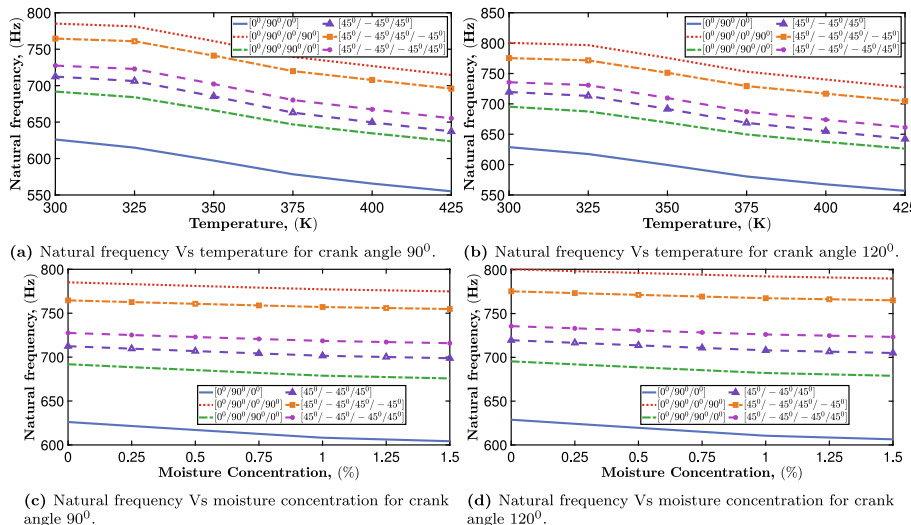
Table 9
Fundamental frequencies (Hz) for one-fold plate with increase in temperature (K)

Crank angle	Lamination scheme	h (mm)	Source	Temperature					
				300 K	325 K	350 K	375 K	400 K	425 K
90°	$[0^\circ/90^\circ]_2$	7	Present	59.247	46.89	32.14			
			Das and Niyogi [68]	59.83	47.49	32.97	8.91		
			Present	76.042	66.719	57.313	47.686	37.927	23.707
		15	Das and Niyogi [68]	76.54	67.25	57.92	48.52	39.31	26.78
			Present	125.86	119.98	114.6	109.68	105.52	101.21
			Das and Niyogi [68]	126.28	120.42	115.06	110.19	106.10	101.88
	$[0^\circ/90^\circ]_s$	7	Present	46.38	28.215	19.875			
			Das and Niyogi [68]	47.10	28.55				
			Present	59.571	46.68	30.862			
		9	Das and Niyogi [68]	60.17	47.15	31.22			
			Present	98.855	90.975	83.535	76.416	70.016	62.975
			Das and Niyogi [68]	99.35	91.45	83.97	76.83	70.42	63.38
120°	$[0^\circ/90^\circ]_2$	7	Present	59.296	47.251	32.97	8.7274		
			Das and Niyogi [68]	59.85	47.86	33.77	11.63		
			Present	76.125	67.021	57.85	48.496	39.088	25.733
		9	Das and Niyogi [68]	76.59	67.52	58.38	49.11	39.88	27.02
			Present	126.1	120.33	115.06	110.24	106.16	101.94
			Das and Niyogi [68]	126.46	120.70	115.42	110.59	106.51	102.30
	$[0^\circ/90^\circ]_s$	7	Present	46.381	28.551	18.648			
			Das and Niyogi [68]	47.08	29.18				
			Present	59.573	46.918	31.387			
		9	Das and Niyogi [68]	60.15	47.49	32.04			
			Present	98.863	91.116	83.798	76.789	70.484	63.553
			Das and Niyogi [68]	99.33	91.59	84.26	77.24	70.95	64.04
180°	$[0^\circ/90^\circ]_2$	7	Present	28.747	14.773				
			Das and Niyogi [68]	28.89	15.01				
			Present	36.94	27.473	14.592			
		9	Das and Niyogi [68]	37.06	27.62	14.81			
			Present	61.414	55.995	50.787	45.812	41.302	36.083
			Das and Niyogi [68]	61.49	56.08	50.87	45.90	41.39	36.18
	$[0^\circ/90^\circ]_s$	7	Present	30.853	18.422				
			Das and Niyogi [68]	31.00	18.63				
			Present	39.63	31.043	20.121			
		9	Das and Niyogi [68]	39.75	31.18	20.33			
			Present	65.759	60.845	56.111	51.643	47.663	43.095
			Das and Niyogi [68]	65.90	60.99	56.27	51.81	47.84	43.29

Table 10

Fundamental frequencies (Hz) for one-fold plate at increased moisture concentration (%)

Crank angle	Lamination scheme	h (mm)	Source	Moisture (%)						
				0	0.25	0.5	0.75	1	1.25	1.5
90°	[0°/90°] ₂	7	Present	59.247	31.401					
			Das and Niyogi [68]	59.83	32.20					
		9	Present	76.042	57.353	28.952				
			Das and Niyogi [68]	76.54	57.95	30.31				
			Present	125.86	115.59	104.81	93.362	80.96	64.836	42.56
	[0°/90°] _s	7	Das and Niyogi [68]	126.28	116.06	105.38	94.09	81.93	66.21	44.90
			Present	46.38	19.837					
		9	Das and Niyogi [68]	47.10						
			Present	59.571	31.021					
			Das and Niyogi [68]	60.17	31.42					
120°	[0°/90°] ₂	7	Present	98.855	84.942	68.772	48.06			
			Das and Niyogi [68]	99.35	85.39	69.21	48.56			
		9	Present	59.296	32.29					
			Das and Niyogi [68]	59.85	33.16					
			Present	76.125	57.912	30.672				
	[0°/90°] _s	15	Das and Niyogi [68]	76.59	58.48	31.88				
			Present	126.1	116.06	105.54	94.365	82.305	66.738	45.682
		15	Das and Niyogi [68]	126.46	116.44	105.94	94.83	82.85	67.46	46.84
			Present	46.381	18.575					
			Das and Niyogi [68]	47.08						
180°	[0°/90°] ₂	7	Present	59.573	31.577					
			Das and Niyogi [68]	60.15	32.29					
		9	Present	98.863	85.216	69.331	49.018	6.4195		
			Das and Niyogi [68]	99.33	85.69	69.86	49.75	10.80		
			Present	28.747						
	[0°/90°] _s	9	Das and Niyogi [68]	28.89						
			Present	36.94	13.695					
		15	Das and Niyogi [68]	37.06	13.95					
			Present	61.414	51.071	38.566	20.189			
			Das and Niyogi [68]	61.49	51.16	38.67	20.38			

**Fig. 5.** Frequency variation of one-fold folded laminated composite plate under uniform distribution of thermal and moisture for CCCC boundary condition.

Tables 11 and 12. The obtained frequencies are compared with the available results of Das and Niyogi [68] and found to be performing better as the natural frequency are less than the available FSDT solution of Das and Niyogi [68] which over-predicts the frequency. Further, it is observed that, unlike one-fold folded plate, the two-fold

folded laminated composite plates have a significant difference in the natural frequency with a different crank angle like $\beta = 90^\circ, 120^\circ$ due to prominent bending-extensional coupling in the two-fold folded plate. However, the increase in stiffness due to two-fold is compensated by the depreciation in stiffness due to thermal and moisture

Table 11

Fundamental frequencies (Hz) for two-fold folded plate with increase in temperature (K)

Crank angle	Lamination scheme	h (mm)	Source	Temperature					
				300 K	325 K	350 K	375 K	400 K	425 K
90°	[0°/90°] ₂	7	Present	50.427	38.748	18.413			
			Das and Niyogi [68]	50.69	39.03	18.83			
			Present	64.729	56.463	46.585	34.344	17.007	
		15	Das and Niyogi [68]	64.91	56.64	46.72	34.43	17.05	
			Present	107.21	102.24	97.453	92.863	88.824	84.445
			Das and Niyogi [68]	107.24	102.28	97.45	92.83	88.77	84.35
	[0°/90°] _s	7	Present	41.748	23.595				
			Das and Niyogi [68]	42.14	24.06				
			Present	53.624	42.613	22.733			
		15	Das and Niyogi [68]	53.93	42.88	22.96			
			Present	88.996	83.018	76.665	69.924	63.295	55.183
			Das and Niyogi [68]	89.22	83.24	76.83	70.00	63.28	55.01
120°	[0°/90°] ₂	7	Present	64.305	56.139	45.904	21.315		
			Das and Niyogi [68]	64.48	56.29	46.16	25.67		
			Present	82.522	76.496	70.105	63.431	54.989	39.747
		15	Das and Niyogi [68]	82.65	76.60	70.18	63.52	56.39	41.62
			Present	136.38	132.78	129.23	125.96	123.2	120.24
			Das and Niyogi [68]	136.54	132.94	129.38	126.09	123.35	120.40
	[0°/90°] _s	7	Present	50.48	38.678	17.634			
			Das and Niyogi [68]	50.74	38.93	17.94			
			Present	64.815	56.482	46.446	33.883	15.391	
		15	Das and Niyogi [68]	64.99	56.65	46.56	33.77	11.35	
			Present	107.45	102.48	97.623	92.984	88.902	84.451
			Das and Niyogi [68]	107.48	102.49	97.63	92.95	88.81	84.22

effects. Therefore, the same thing is observed for moisture variation as shown in Table 12.

After the validation of the result for the two-fold folded laminated composite plate, the pattern of variation of natural frequency with respect to the temperature and moisture for cross-ply and angle-ply laminate is evaluated and shown in Fig. 6. In this case the side-to-thickness ratio, $a/h = 10$ has been considered. It is observed that, unlike one-fold folded plate, the two-fold folded plate shows a significant variation with change in crank angle from $\beta = 90^\circ$ to $\beta = 120^\circ$ for various temperature and moisture.

3.5. Transient analysis

In this section, the transient analyses of flat and folded laminated composite plates under the hygrothermal environment are extensively carried out. Firstly, the transient displacement analysis along with Rayleigh damping consideration for flat laminated composite plate is carried out, then the transient responses of the one-fold and two-fold folded laminated composite plate are investigated, and at last, the transient stresses of the laminated composite plate are evaluated for various types of loads and boundary conditions under hygrothermal load. The present approach is first validated with the available solution in the literature, then some novel interpretations and insights are presented. Some problems have been verified with ANSYS software solutions and those solutions have been obtained using mesh size (8×8) for one-fold and (9×9) for the two-fold folded plate with the element type, shell 8 node 281.

3.5.1. Simply supported cross-ply laminated composite plate under UDL with temperature dependent material properties

The present transient analysis approach is validated with the available solution in the literature. To do so, a twenty-layered $[0^\circ/90^\circ]_{10}$ cross-ply laminated composite plate with dimensions, $a = b = 0.5\text{ m}$, and $h = 5\text{ mm}$, is considered. The plate is made of temperature-dependent material properties as given in MM3. A uniform change in temperature, $\Delta T = T - 300 = \text{constant}$, is employed under simply supported (SSSS-1) boundary condition. Then a uniformly distributed transverse step load with magnitude, $P_0 = 100\text{ N/m}^2$, for time, $t_1 = 0.03\text{ s}$, is applied to the plate. The results are obtained by taking a time step, $\Delta t = 10^{-6}\text{ s}$. The obtained results for $T = 300\text{ K}$ and $T = 400\text{ K}$ are shown in Fig. 7a. The solutions have also been obtained by ANSYS APDL and presented in Fig. 7a, which is found to be in good agreement with the present solution. The same problem is also analyzed for the moisture concentration, $C = 0\%$, and $C = 1\%$, and obtained solutions are shown in Fig. 7b. The obtained results are in good agreement with the available one from the Parhi et al. [15]. The increase in temperature and moisture increases the central deflection and decreases the natural frequency due to a decrease in stiffness of the structure under the hygrothermal effect. Moreover, due to the utilization of higher-order shear deformation theory, the present responses are found to be better. Also, due to the adverse effect of the hygrothermal load on the stiffness, the responses for the hygrothermal load are significantly different from the one without them, which makes it essential to have a proper hygrothermal analysis to deal with practical problem arose due to the hygrothermal environment.

Table 12

Fundamental frequencies (Hz) for two-fold folded plate with increase in moisture concentration (%).

Crank angle	Lamination scheme	h (mm)	Source	Moisture (%)						
				0	0.25	0.5	0.75	1	1.25	1.5
90°	[0°/90°] ₂	7	Present	50.427	16.532					
			Das and Niyogi [68]	50.69	17.05					
			Present	64.729	46.477					
		15	Das and Niyogi [68]	64.91	46.63					
			Present	107.21	98.348	87.873	75.264	59.343	31.457	
			Das and Niyogi [68]	107.24	98.36	87.85	75.13	59.03	30.51	
	[0°/90°] _s	7	Present	41.748						
			Das and Niyogi [68]	42.14						
			Present	53.624	22.291					
		15	Das and Niyogi [68]	53.93	22.58					
			Present	88.996	77.792	60.954	31.444			
			Das and Niyogi [68]	89.22	77.96	60.91	30.53			
120°	[0°/90°] ₂	7	Present	64.306	45.158					
			Das and Niyogi [68]	64.48	45.44					
			Present	82.522	69.871	46.861				
		15	Das and Niyogi [68]	82.65	69.96	49.06				
			Present	136.38	129.63	122.34	114.42	105.73	94.164	70.89
			Das and Niyogi [68]	136.54	129.77	122.46	114.52	105.83	94.32	72.06
	[0°/90°] _s	7	Present	50.48	15.588					
			Das and Niyogi [68]	50.74	15.99					
			Present	64.815	46.327					
		15	Das and Niyogi [68]	64.99	46.47					
			Present	107.45	98.515	87.927	75.068	58.708	29.156	
			Das and Niyogi [68]	107.48	98.53	87.88	74.86	58.05	26.25	

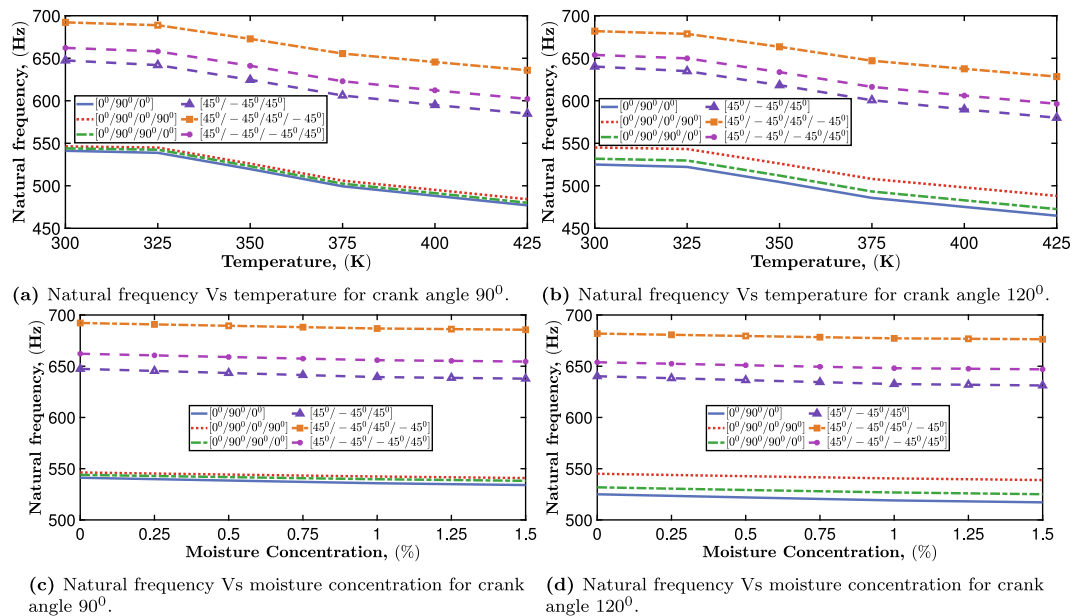


Fig. 6. Frequency variation of two-fold laminated composite plate under uniform distribution of thermal and moisture for CCCC boundary condition.

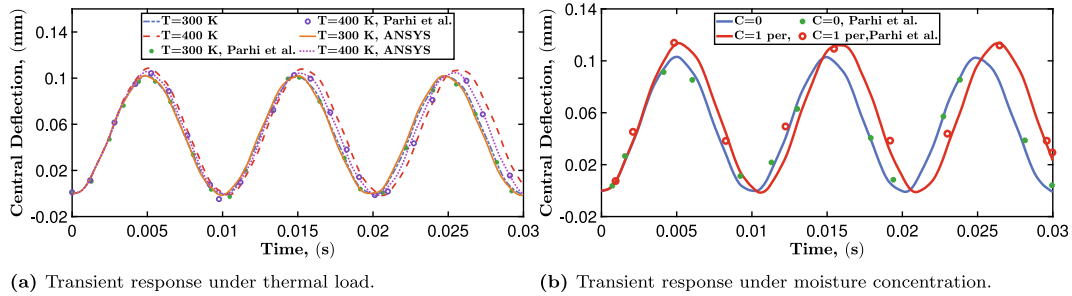


Fig. 7. Transient response of central deflection of laminated composite plate under SSSS-1 boundary condition for uniformly distributed load, 100 N/m^2 , with thermal and moisture load.

3.5.2. Effect of thermal environment on the transient response due to various types of mechanical loading

To assess the effect of various types of time-dependent loading on the laminated composite plate under the hydrothermal environment, a three-layered $[0^0/90^0/0^0]$ cross-ply laminated composite plate with dimensions, $a = b = 0.5 \text{ m}$, and thickness, $h = 5 \text{ mm}$, is again considered. The uniformly distributed, $\Delta T = T_0$, and sinusoidally distributed, $\Delta T = T_0 \sin(\frac{\pi x}{a}) \sin(\frac{\pi y}{b})$, change in temperature, are considered with temperature-dependent material properties MM3. The uniformly distributed transverse load with magnitude, $P_0 = 100 \text{ N/m}^2$, is employed. The various types of load, such as step, sinusoidal, exponential, and triangular loads, are applied for $t_1 = 0.03 \text{ s}$, under simply supported boundary condition (SSSS-1). The time step used for the Newmark's scheme is $\Delta t = 10^{-5} \text{ s}$. The response is obtained for $T = 300 \text{ K}$ and $T = 400 \text{ K}$ in the case of UDL thermal load while $T = 350 \text{ K}$ and $T = 400 \text{ K}$ in the case of SSL thermal load. The obtained solutions are shown in Fig. 8. It is observed in the figure that the difference between the response of SSL thermal load is more than the UDL thermal load due to SSL thermal load being more adversely affecting the centre of the plate with high intensity than the UDL thermal load.

The same problem is also studied for the sinusoidally distributed transverse loading, and the obtained solutions are shown in Fig. 9. Also, in this case, the same pattern is observed due to SSL thermal load being more adversely affecting the laminated composite plate at the centre. However, the sinusoidal spatial distributed (SSL) mechanical

load caused less deflection than the uniformly distributed (UDL) mechanical load due to less cumulative magnitude in SSL than the UDL spatial load.

3.5.3. Effect of thermal environment on the transient response under various boundary conditions

A cross-ply $[0^0/90^0/0^0]$ plate having dimensions, $a = b = 0.5 \text{ m}$, and $a/h = 50$, is considered. A uniform change in temperature, $\Delta T = T - 300 = \text{constant}$, with material MM3 is taken for the analysis. Transverse sinusoidal load (SSL) applied is having magnitude, $P_0 = 100 \text{ N/m}^2$, with various types of temporal variations such as step load, sinusoidal load, exponential load, and triangular load for time, $t_1 = 0.03 \text{ s}$, and time step is $\Delta t = 10^{-5} \text{ s}$. The transient responses are obtained for $T = 300 \text{ K}$ and $T = 400 \text{ K}$, and shown in Fig. 10. The problem is analyzed to assess the effect of the thermal environment on the response under various boundary conditions. The boundary conditions considered are SSSS-1, SSFS, SSFF, CCFC, and CCFF. It is observed that the boundary condition does affect not only the deflection but also the frequency of the dynamic response due to the varying constraints for different boundary conditions. Moreover, it is also observed that the frequency reduces, and displacement increases after imposition of free boundary conditions due to a decrease in boundary constraints.

Further, the whole plate deflection pattern of the problem mentioned above has been shown in Figs. 11 and 12, for CCFC and CCFF

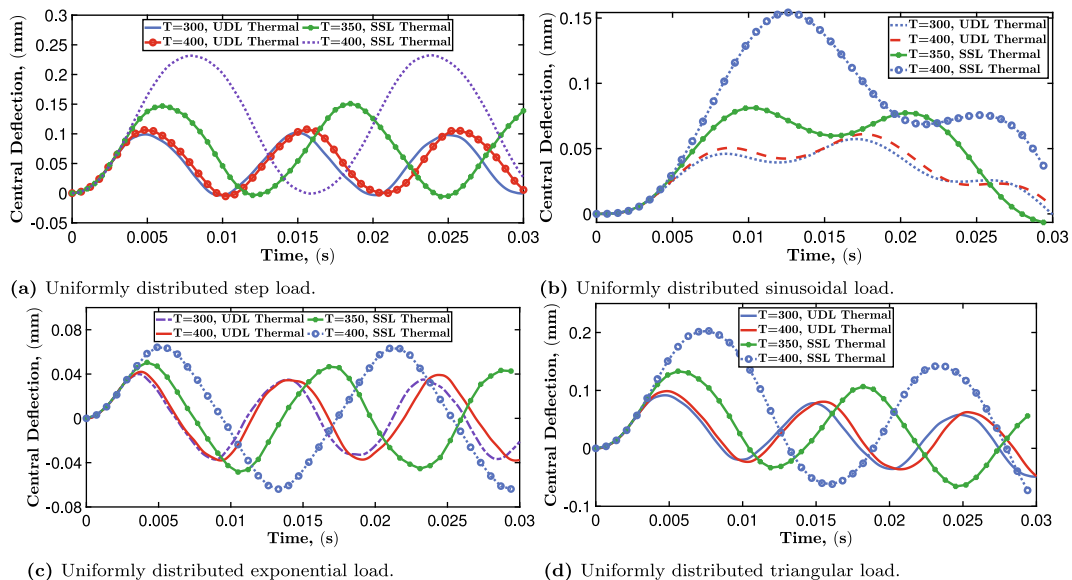


Fig. 8. Transient analysis of laminated composite plate under uniformly distributed spatial load with various types of temporal mechanical load with intensity, 100 N/m^2 , subjected thermal load for SSSS-1 boundary condition.

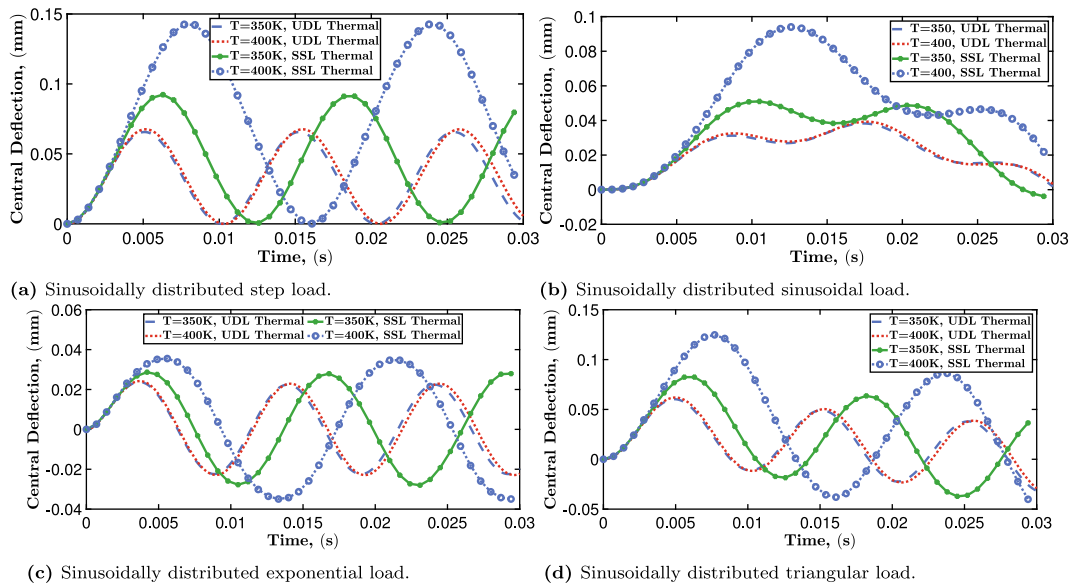


Fig. 9. Transient analysis of laminated composite plate under sinusoidally distributed spatial load with various types of temporal mechanical load with intensity, 100 N/m^2 , and UDL and SSL distribution of thermal load for SSSS-1 boundary condition.

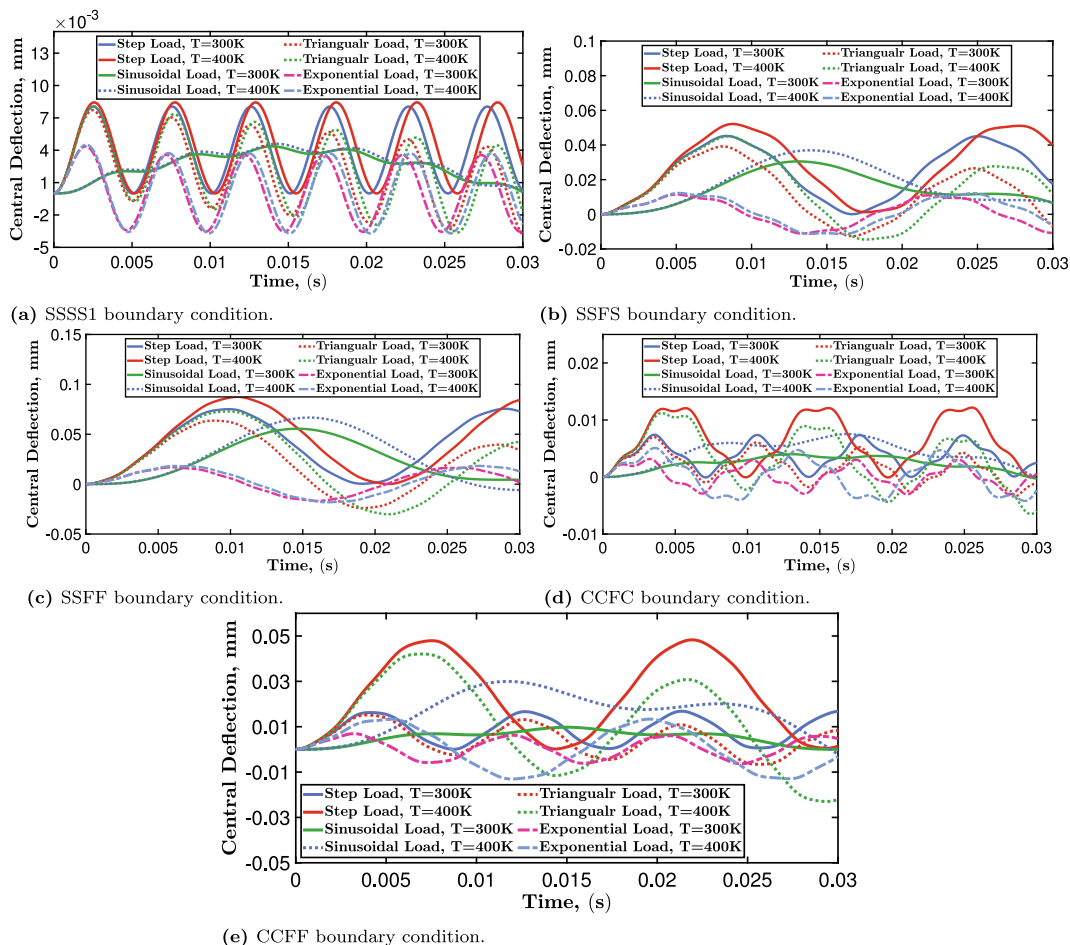


Fig. 10. Effect of various boundary conditions such as SSSS1, SSFS, SSFF, CCFC, and CCFF on the transient central displacement response of three layered laminated composite $[0^\circ/90^\circ/0^\circ]$ plate under thermal load.

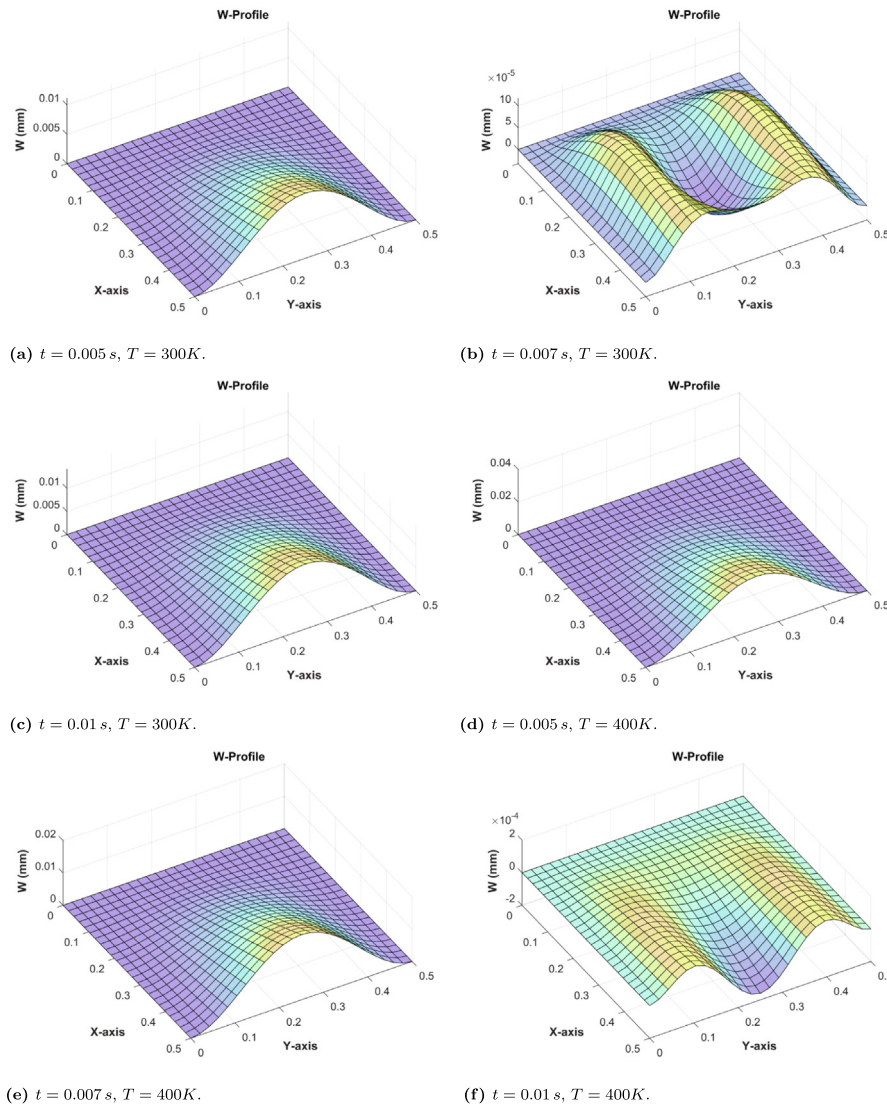


Fig. 11. Whole plate deflection of a cross-ply $[0^\circ/90^\circ/0^\circ]$ plate at different time, t due to time dependent load for CCFC boundary condition.

boundary conditions, respectively. The deflection pattern has been shown for a particular time instance like time, $t = 0.005 \text{ s}, 0.007 \text{ s}$, and 0.01 s for temperature, $T = 300 \text{ K}$ and 400 K . The results shown in Figs. 11 and 12 give an illustration of transient response shown in Fig. 10 for a particular time instance. It demonstrates the pattern of the maximum and minimum central deflection observed in transient response graphically.

3.5.4. Effect of thermal environment on the transient damped response of laminated composite plate

A cross-ply $[0^\circ/90^\circ/90^\circ/0^\circ]$ laminated composite plate is considered for the damped transient analysis, which considers the Rayleigh damping model to incorporate the damping in the system. The plate is made of material MM4 and has side-length, $a = b = 25 \text{ cm}$, and side-to-thickness ratio, $a/h = 10$. The transverse step load, along with

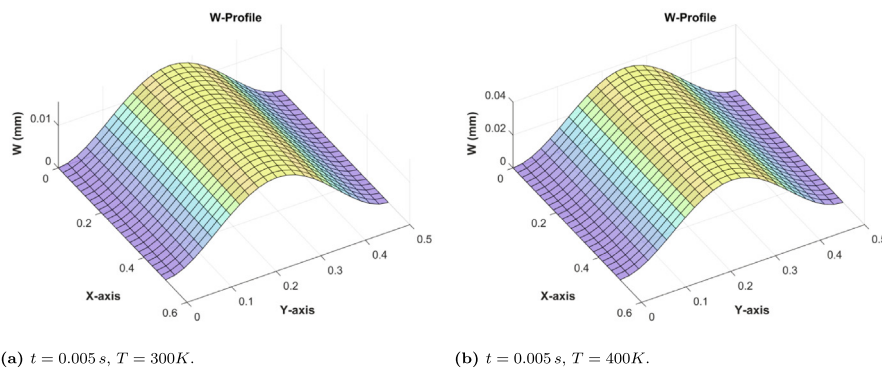


Fig. 12. Whole plate deflection of a cross-ply $[0^\circ/90^\circ/90^\circ/0^\circ]$ plate at differet time, t due to time dependent load for CCFF boundary condition.

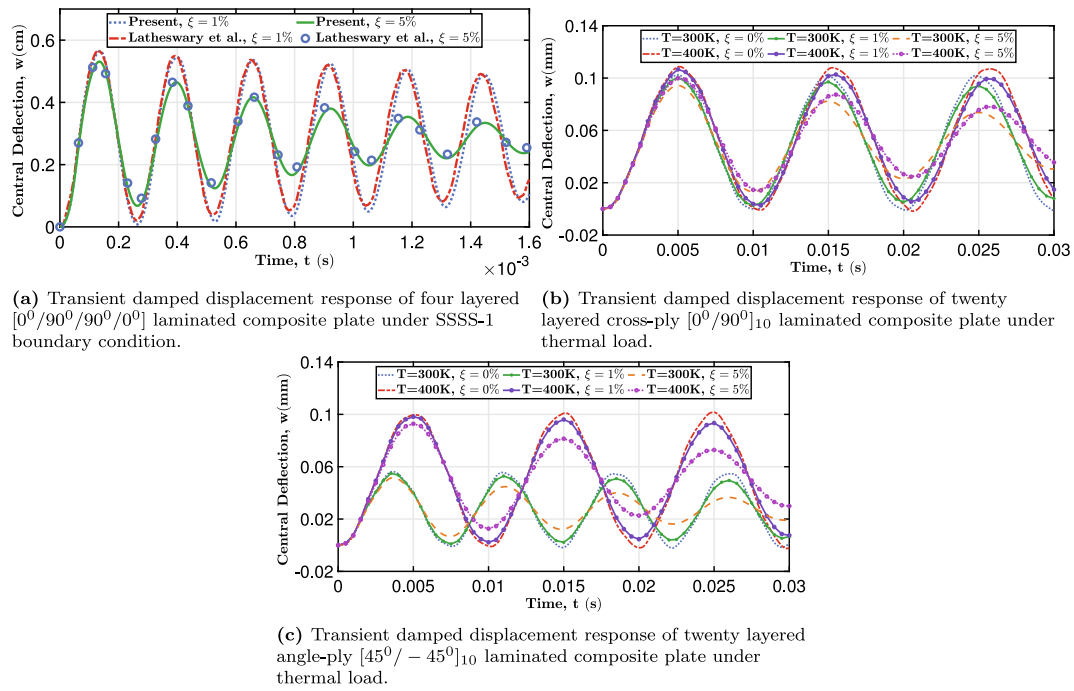


Fig. 13. Transient damped response due to uniformly distributed step load under thermal environment.

uniformly distributed spatial load, is applied for the time, $t_1 = 1.6 \text{ ms}$, and the time-step taken for the analysis is $\Delta t = 10^{-5} \text{ s}$. The applied nondimensional load, $Q = (P_0 b^4)/(E_2 h^4) = 10$, is considered for the analysis under simply supported (SSSS-1) boundary condition. To validate the present approach for the damping analysis, this linear damped transient response is obtained, and the result is validated by the available solution of Latheswary et al. [42] and shown in Fig. 13a. The present solutions are in good agreement with the available ones.

Then a laminated composite plate with dimensions as $a = b = 0.5 \text{ m}$, and thickness $h = 5 \text{ mm}$, is considered for the damped response under thermal load. The damped response for damping factor, $\xi = 0\%$, $\xi = 1\%$, and $\xi = 5\%$, under thermal and mechanical load with magnitude, $P_0 = 100 \text{ N/m}^2$, has been obtained for the twenty layered cross-ply $[0^\circ/90^\circ]_{10}$ laminated composite plate having material properties MM3, and the obtained responses are shown in the Fig. 13b. Further, the damped response of twenty layered angle-ply $[45^\circ/-45^\circ]_{10}$ laminated composite plate has also been obtained and shown in Fig. 13c. It is observed that the difference in the response

for different temperatures, $T = 300 \text{ K}$ and 400 K are more in the angle-ply than the cross-ply.

3.5.5. Validation of transient response of folded laminated composite plate

In this subsection, the present formulation is validated for the transient analysis of one-fold and two-fold folded cantilever laminated $[30^\circ/-30^\circ]$ composite plate. The plate is made of material MM2 and has dimensions as $a = b = 1.5 \text{ m}$ and $a/h = 50$. A transverse step load with intensity $1 \times 10^5 \text{ N/m}^2$ is applied for $t_1 = 0.01 \text{ s}$. The central tip deflection responses of one-fold and two-fold are obtained for various fold-angle using $\Delta t = 5 \times 10^{-6} \text{ s}$ and shown in Fig. 14. The obtained response has been compared with the available results of Niyogi et al. [49] and the ANSYS solution and are found to be in good agreement. The central tip (point B in Fig. 2a) deflection response of one-fold folded cantilever laminated composite plate for the fold-angle 90° and 120° is shown in Fig. 14a. A little difference is observed in the response of ANSYS and present FEM solution due to the utilization of FSDT in ANSYS software. It is observed that with an increase in fold angle, the rigidity of the structure decreases. Further, the transient

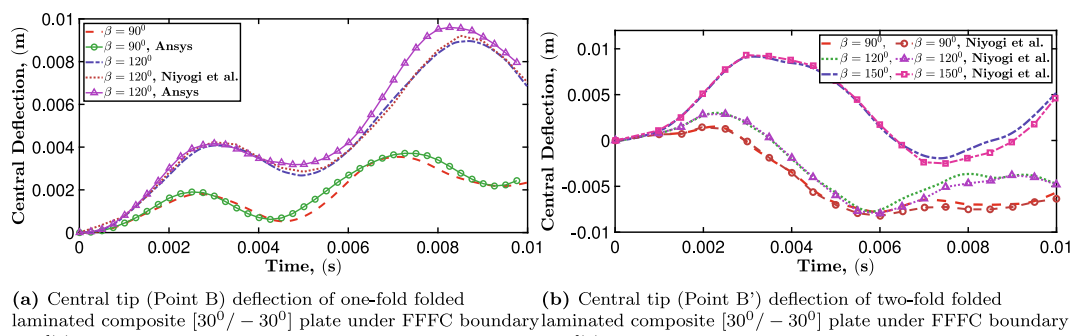


Fig. 14. Central tip deflection of onefold and twofold folded laminated composite plate under uniformly distributed load of magnitude 10^5 N/m^2 for FFFC boundary condition.

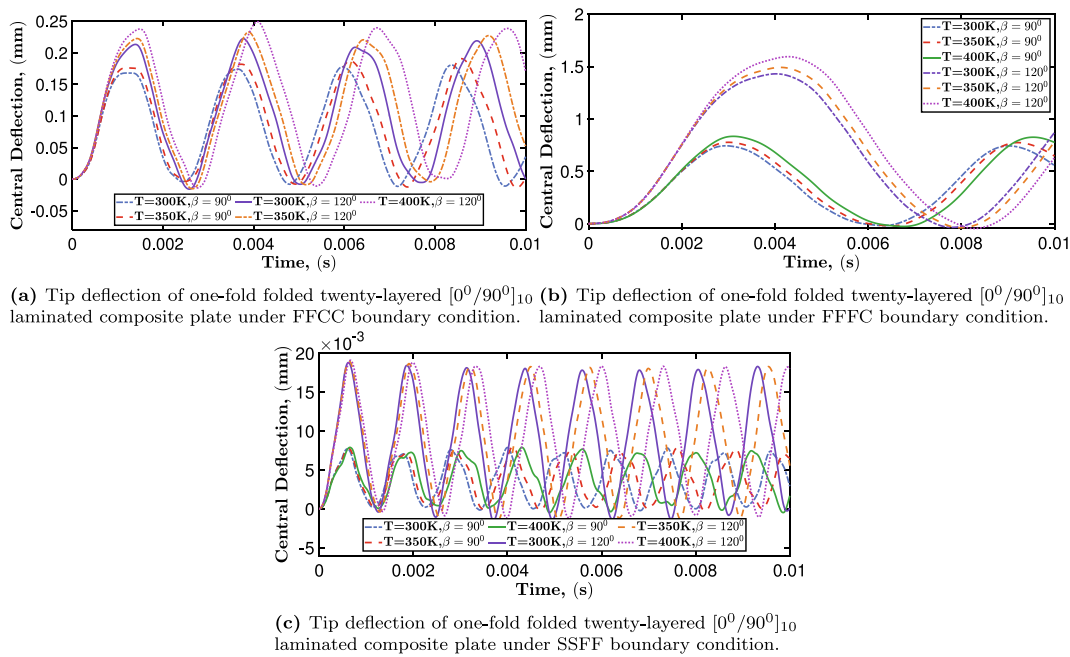


Fig. 15. Tip deflection of one-fold folded twenty-layered $[0^\circ/90^\circ]_{10}$ laminated composite plate under various boundary conditions and thermal load for applied step load of magnitude 10^5 N/m^2 .

response of two-fold folded cantilever laminated composite plate has also been shown in Fig. 14b for crank angle 90° , 120° and 150° . Here also, it is observed that due to a decrease in flexural rigidity, the central tip (point B' in Fig. 2b) deflection increases with an increase in crank angle.

3.5.6. Transient response of one-fold folded laminated composite plate under hygrothermal environment

For the transient analysis of one-fold folded laminated composite plate under hygrothermal environment, twenty-layered cross-ply

$[0^\circ/90^\circ]_{10}$ laminated composite plate with crank angle 90° and 120° is considered as shown in Fig. 2a. The plate has dimensions as $a = b = 1.5\text{m}$, and side-to-thickness ratio, $a/h = 10$. The material used for the analysis is MM5. The transient response under hygrothermal environment is obtained for the applied load $P = 10^5 \text{ N/m}^2$ at temperature, $T = 300 \text{ K}$, 350 K and 400 K . The step load is applied for $t_1 = 0.01 \text{ s}$. The responses of the tip point (Point B , $x = a/2, y = b/2$ in flat plate) deflection for FFFC (one folded side clamped), FFCC (both folded side clamped) and SSFF (both unfolded side immovable simply supported) boundary conditions are shown in Fig. 15. It is observed

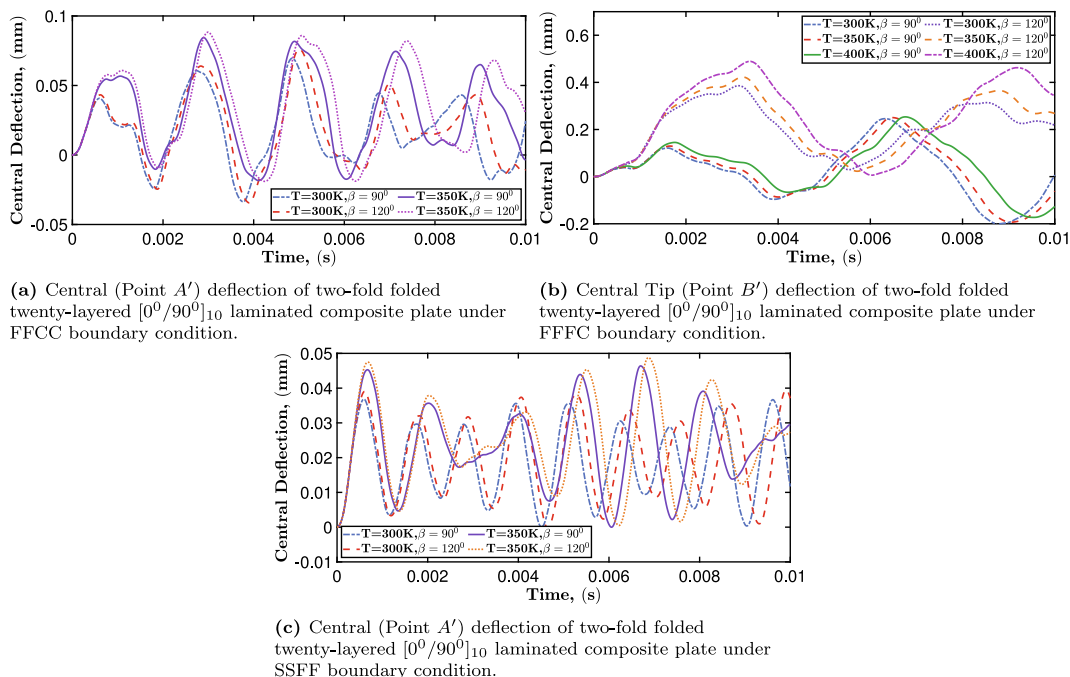


Fig. 16. Tip and central deflection of twofold folded twenty-layered $[0^\circ/90^\circ]_{10}$ laminated composite plate under various boundary conditions and thermal load for applied step load of magnitude 10^5 N/m^2 .

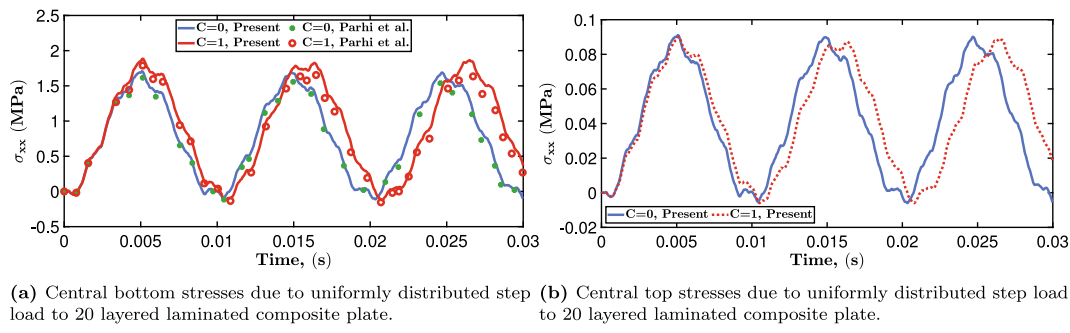


Fig. 17. Transient stress under uniformly distributed step load with intensity 100 N/m^2 and UDL hygral load with moisture $C = 0\%$ and $C = 1\%$ for SSSS-1 boundary condition.

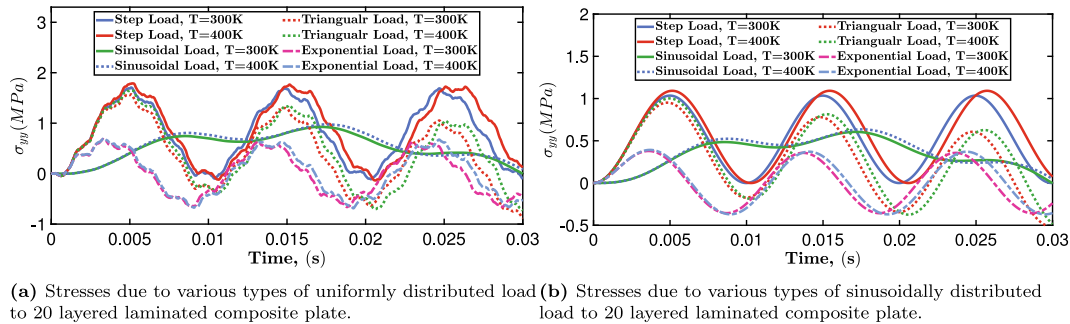


Fig. 18. Transient stress ($\sigma_{yy}(a/2, b/2, h/2)$) under UDL and SSL types of load with intensity 100 N/m^2 and UDL thermal load with temperature $T = 300 \text{ K}$ and $T = 400 \text{ K}$ for SSSS-1 boundary condition.

that the boundary conditions have a prominent effect on the transient response of folded laminated composite plates. Apart from boundary conditions, the crank angle also plays an important role with varying temperature. Fig. 15a shows the displacement response for FFCC boundary condition and has large frequency and less amplitude than the FFFC boundary condition shown in Fig. 15b. This is due to more constraints in the case of both folded sides clamped (FFCC). However, the frequency is much greater and deflection is lesser in the case of SSFF boundary condition as shown in Fig. 15c.

3.5.7. Transient response of two-fold folded laminated composite plate under thermal environment

For the analysis of two-fold folded laminated composite plate under hygrothermal environment, twenty-layered cross-ply $[0^\circ/90^\circ]_{10}$ laminated composite plate with crank angle 90° and 120° is considered as shown in Fig. 2b. The plate has dimensions as $a = 1.5 \text{ m}$, $b = 2.25 \text{ m}$, and side-to-thickness ratio, $a/h = 10$. The material used for the analysis is MM5. The transient response under hygrothermal environment is obtained for the applied load $P = 10^5 \text{ N/m}^2$ at temperature, $T = 300 \text{ K}$, 350 K and 400 K . The step load is applied for $t_1 = 0.01 \text{ s}$. The responses of the tip (Point B' , $x = a$, $y = b/2$ in flat plate) deflection for FFCC (both folded side clamped) and FFFC (one folded side clamped), and the central (Point A' , $x = a/2$, $y = b/2$ in flat plate) deflection for the SSFF (both unfolded side immovable simply supported) boundary conditions are shown in Fig. 16. It is observed that the effect of various boundary conditions is even greater in the two-fold folded plate than the one-fold folded plate. Moreover, the response seems to be more complex due to the combined effect of folding and thermal load. Here, the responses of the FFCC and SSFF have only been shown for the temperature, $T = 300 \text{ K}$ and $T = 350 \text{ K}$ as the response at $T = 400 \text{ K}$ gets unstable in the case of FFCC and SSFF, however, in the case of FFFC boundary

condition, the response for temperature, $T = 400 \text{ K}$ has also been shown.

3.5.8. Transient stress response

The stresses in the structure play an important role in the design and manufacturing; hence, they need to be analyzed for the hygrothermal environment. In this section, dynamic normal stresses have been calculated for the twenty layered $[0^\circ/90^\circ]_{10}$ laminated composite plate having material property MM3 under SSSS-1 boundary condition. The normal stresses, σ_{xx} and σ_{yy} have been evaluated at the centre top and bottom surfaces, and the obtained responses are shown in Figs. 17 and 18. Fig. 17a shows the effect of moisture on the dynamic response of central bottom surface stress ($-\sigma_{xx}(a/2, b/2, -h/2)$), and found to be in well agreement with the Parhi et al. [15]. Whereas, Fig. 17b shows the moisture concentration effect on the transient stress ($\sigma_{xx}(a/2, b/2, h/2)$) response of central top surface. It is observed that the top and bottom surface stresses are significantly different due to the anti-symmetric orientation of the laminae. Further, the dynamic stress ($\sigma_{yy}(a/2, b/2, h/2)$) response due to various type of uniformly distributed mechanical load under thermal load are obtained and shown in Fig. 18a. Moreover, the same response is obtained for the sinusoidal mechanical loading, and the obtained responses are shown in Fig. 18b.

3.6. Steady state analysis

In this section, linear harmonic analysis under hygrothermal environment is carried out for various parameters. The linear frequency response in the neighborhood of natural frequency is obtained. The solutions have been obtained by the MATLAB finite element code as well as with the ANSYS mechanical APDL for validation purposes. The ANSYS solution has been obtained using a mesh size of (8×8)

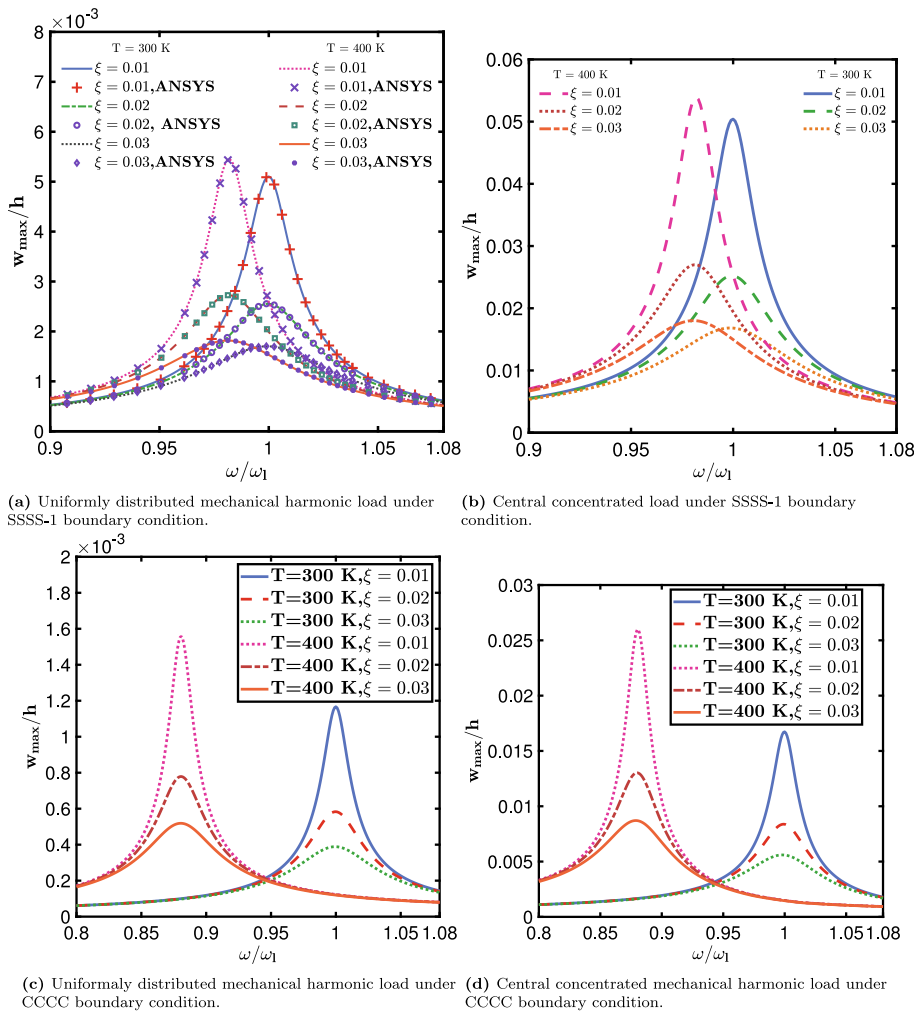


Fig. 19. Effect of various boundary conditions and harmonic load on the frequency response of three layered laminated composite $[0^{\circ}/90^{\circ}/0^{\circ}]$ plate under thermal load.

with shell 8 node 281 element type. Also, to incorporate the stress stiffening effect due to thermal load, Green–Lagrange strain–displacement relationship has been used.

3.6.1. Steady state analysis of three-layered cross-ply laminated composite plate

A three-layered cross-ply $[0^{\circ}/90^{\circ}/0^{\circ}]$ laminated composite plate having material properties MM3 is taken for the harmonic analysis under the hygrothermal environment. A transverse harmonic force, $P = P_0 \cos(\omega t)$, with magnitude, $P_0 = 1 \text{ N/m}^2$, is applied to the plate. Also, the steady-state response for concentrated load with a magnitude, $P = 1 \text{ N}$, is obtained. The frequency response in the neighborhood of natural frequency for SSSS-1 and CCCC boundary conditions is shown in Fig. 19. The ANSYS APDL solutions have also been obtained to validate the thermal effect on the harmonic response, and they are found to be well-matched with the present MATLAB finite element formulation for different damping factors and thermal load as shown in Fig. 19a. The Rayleigh damping approach is employed to incorporate the damping parameters, and the same damping parameters are feed into the ANSYS for the solution. It is observed that the uniform distribution of load produces less deflection amplitude than the concentrated load for both SSSS-1 and CCCC boundary conditions. Moreover, the peak amplitude for elevated temperature ($T = 400 \text{ K}$) is found at less than the natural frequency (ω_l) as an increase in temperature reduces the stiffening effect of the composite laminate, and

hence decreases the frequency. Further, the difference in the frequency ratio (ω/ω_l) at which the peak deflection is observed for $T = 300 \text{ K}$ and $T = 400 \text{ K}$ is larger in the CCCC boundary condition than the SSSS-1 boundary condition due to more constraints effect in the clamped boundary condition.

It can be observed in the Fig. 19 that the increase in thermal load decreases the frequency and increases the deflection as the peak amplitude ratio (W_{max}/h) is higher for the $T = 400 \text{ K}$ than the $T = 300 \text{ K}$. Moreover, the boundary condition is also contributing significantly as the response for the CCCC boundary condition shows a large frequency variation than the SSSS-1 boundary condition due to a more stiffening effect in the CCCC boundary condition. Further, the central concentrated load has also been considered and the obtained responses are shown in Figs. 19b and 19d.

3.6.2. Steady state analysis of twenty-layered laminated composite plate

The twenty-layered cross-ply $[0^{\circ}/90^{\circ}]_{10}$ and angle-ply $[45^{\circ}/-45^{\circ}]_{10}$ laminated composite plate, which has been considered in Section 3.5.4 for transient damped analysis, are also considered for the harmonic response. The frequency response for the laminated composite plate having dimensions, $a = b = 0.5 \text{ m}$, and $h = 5 \text{ mm}$, in the neighborhood of natural frequency is obtained and shown in Fig. 20. The response shown in the figure is for damping factor, 1%, 2%, and 3%, subjected to uniformly distributed and central concentrated harmonic load with magnitude, 1 N/m^2 , and 1 N , respec-

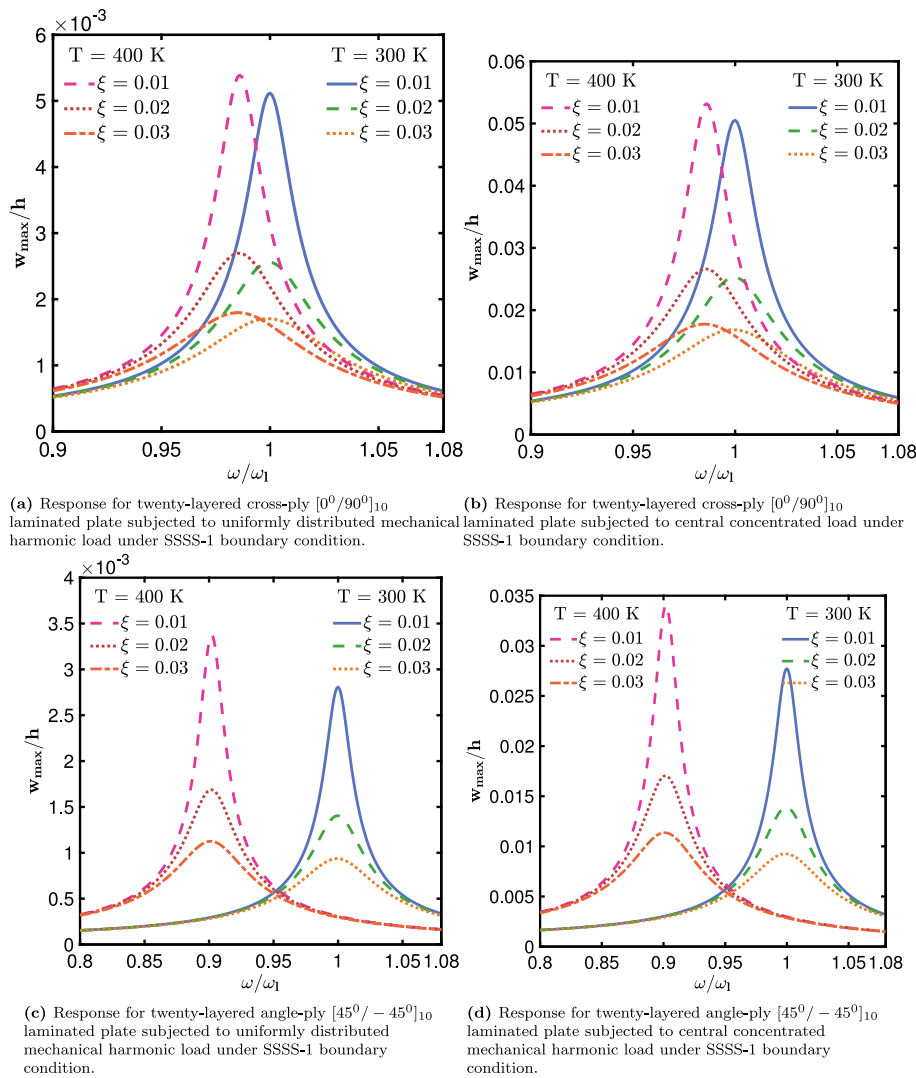


Fig. 20. Frequency response of twenty-layered cross-ply $[0^\circ/90^\circ]_{10}$ and angle-ply $[45^\circ/-45^\circ]_{10}$ laminated composite plate under harmonic uniformly distributed and pointed load with magnitude, 1 N/m^2 , and 1 N , respectively, under SSSS-1 boundary condition.

tively. It can be observed from the Fig. 20 that the difference in peak amplitude ratio for $T = 300 \text{ K}$ and $T = 400 \text{ K}$ is more in the angle-ply than the cross-ply due to an increase in stiffening effect in the case of angle-ply laminate. Further, the deflection amplitude ratio for angle-ply is less than the cross-ply due to the same reason. Moreover, like the previous example, the central concentrated load again causes more deflection amplitude than the uniformly distributed load, hence, the nature of load applied, even with the same magnitude, is critical for the structural behavior.

4. Conclusion

In this paper, as per the author's knowledge, for the first time, the free and forced vibration analysis of flat and folded laminated composite plate under the hygrothermal environment is investigated using a nonpolynomial shear deformation theory. The sinusoidally and uniformly distributed thermal loads are considered to best fit the practical cases found in structural engineering. Moreover, various types of time-dependent loading such as sinusoidal, triangular, exponential, and step loading are applied to evaluate the transient response and get an essential idea about the pertinent behavior of the structure under the

hygrothermal environment. Subspace iteration for the eigenvalue problem and Newmark's scheme for the initial value problem is utilized along with harmonic response for the steady-state solution. Moreover, the damped transient response has also been carried out for the hygrothermal environment. The Rayleigh damped model is incorporated to model the damping parameters.

The present formulation is first validated by comparing the obtained solution with the available 3D elasticity solution for free vibration without the consideration of the hygrothermal environment. Then the hygrothermal effects are considered, and extensive free vibration analyses are carried out for various parameters. The effect of hygrothermal load on the angle-ply laminate seems to be more susceptible than the cross-ply laminate. Further, the effect of various parameters such as thermal and moisture loads is analyzed and observed that the natural frequency of three-layered and four-layered symmetric cross-ply laminate is found to be almost the same due to the absence of the extensional-bending coupling. In contrast to the cross-ply, the angle-ply laminate shows a different pattern and is highly influenced by the lamination scheme.

Further, the transient analysis due to uniformly and sinusoidally distributed mechanical and hygrothermal load is carried out. It is

observed that sinusoidal spatial load causes less deflection than the uniformly distributed load due to less overall magnitude in the case of SSL, whereas, the SSL thermal load produces more deflection due to high thermal magnitude in the centre of the plate. The boundary condition also plays a critical role in the response; for instance, the free boundary allows more deflection due to reduced constraints. Further, the normal stresses play a very critical role in the structure; hence, the transient stresses have been evaluated for cross-ply and angle-ply laminated plates. Further, the steady-state response around the neighborhood of natural frequency has also been obtained under different thermal load and damping factors. The present work illustrates a holistic understanding of the dynamic behavior of laminated composite flat and folded plates under the hygrothermal environment, which can be relied upon for further benchmark analysis pertaining to higher-order shear deformation theory.

Appendix A. The expression for $A_b\phi_b$ and $A_s\phi_s$

$$A_s \phi_s = \begin{bmatrix} 0 & \phi_x & 0 & \phi_y & 0 & 0 & 0 & 0 & 0 & 0 & 0 & 0 & 0 \\ \phi_x & 0 & \phi_y & 0 & 0 & 0 & 0 & 0 & 0 & 0 & 0 & 0 & 0 \\ 0 & 0 & 0 & 0 & 0 & \phi_x & 0 & \phi_y & 0 & 0 & 0 & 0 & 0 \\ 0 & 0 & 0 & 0 & \phi_x & 0 & \phi_y & 0 & 0 & 0 & 0 & 0 & 0 \\ 0 & 0 & 0 & 0 & 0 & 0 & 0 & 0 & 0 & 0 & \phi_x & 0 & \phi_y \\ 0 & 0 & 0 & 0 & 0 & 0 & 0 & 0 & 0 & \phi_x & 0 & \phi_y & 0 \\ 0 & \theta_x & 0 & \theta_y & 0 & 0 & 0 & 0 & 0 & 0 & 0 & 0 & 0 \\ \theta_x & 0 & \theta_y & 0 & 0 & 0 & 0 & 0 & 0 & 0 & 0 & 0 & 0 \\ 0 & 0 & 0 & 0 & 0 & 0 & \theta_x & 0 & \theta_y & 0 & 0 & 0 & 0 \\ 0 & 0 & 0 & 0 & 0 & \theta_x & 0 & \theta_y & 0 & 0 & 0 & 0 & 0 \\ 0 & 0 & 0 & 0 & 0 & 0 & 0 & 0 & 0 & 0 & \theta_x & 0 & \theta_y \\ 0 & 0 & 0 & 0 & 0 & 0 & 0 & 0 & 0 & \theta_x & 0 & \theta_y & 0 \end{bmatrix}$$

CRediT authorship contribution statement

Babu Ranjan Thakur: Conceptualization, Methodology, Data curation, Visualization, Writing - original draft. **Surendra Verma:** Conceptualization, Methodology, Visualization, Writing - original draft. **B.N. Singh:** Conceptualization, Supervision, Writing - review & editing. **D.K. Maiti:** Conceptualization, Supervision, Writing - review & editing.

Declaration of Competing Interest

The authors declare that they have no known competing financial interests or personal relationships that could have appeared to influence the work reported in this paper.

Appendix B. The in-plane stress resultants

$$\begin{bmatrix} N_{xx} & M_{xx} & P_{xx} & R_{xx} & L_{xx} & V_{xx} \\ N_{yy} & M_{yy} & P_{yy} & R_{yy} & L_{yy} & V_{yy} \\ N_{xy} & M_{xy} & P_{xy} & R_{xy} & L_{xy} & V_{xy} \end{bmatrix} = \int_{-\frac{h}{2}}^{\frac{h}{2}} \left\{ \begin{array}{l} \sigma_{mxx} \\ \sigma_{myy} \\ \tau_{mxy} \end{array} \right\} \{ 1 \ z \ f(z) \ zf(z) \ z^2 \ f^2(z) \} dz$$

$$\begin{bmatrix} N_{yz} & M_{yz} & P_{yz} & R_{yz} & L_{yz} & V_{yz} \\ N_{xz} & M_{xz} & P_{xz} & R_{xz} & L_{xz} & V_{xz} \end{bmatrix} = \int_{-\frac{h}{2}}^{\frac{h}{2}} \left\{ \begin{array}{l} \tau_{myz} \\ \tau_{mxz} \end{array} \right\} \{ 1 \ z \ f(z) \ f'(z) \ zf'(z) \ f(z)f'(z) \} dz$$

Appendix C. The expression of B_{bli} , B_{sli} , G_{bnli} , and G_{snli}

$$B_{bli} = \begin{bmatrix} \frac{\partial N_i}{\partial x} & 0 & 0 & 0 & 0 & 0 & 0 \\ 0 & \frac{\partial N_i}{\partial y} & 0 & 0 & 0 & 0 & 0 \\ \frac{\partial N_i}{\partial y} & \frac{\partial N_i}{\partial x} & 0 & 0 & 0 & 0 & 0 \\ 0 & 0 & 0 & \frac{\partial N_i}{\partial x} & 0 & 0 & 0 \\ 0 & 0 & 0 & 0 & \frac{\partial N_i}{\partial y} & 0 & 0 \\ 0 & 0 & 0 & \frac{\partial N_i}{\partial y} & \frac{\partial N_i}{\partial x} & 0 & 0 \\ 0 & 0 & 0 & 0 & 0 & \frac{\partial N_i}{\partial x} & 0 \\ 0 & 0 & 0 & 0 & 0 & 0 & \frac{\partial N_i}{\partial y} \\ 0 & 0 & 0 & 0 & 0 & \frac{\partial N_i}{\partial y} & \frac{\partial N_i}{\partial x} \end{bmatrix}$$

$$B_{sli} = \begin{bmatrix} 0 & 0 & \frac{\partial N_i}{\partial y} & 0 & N_i & 0 & 0 \\ 0 & 0 & \frac{\partial N_i}{\partial x} & N_i & 0 & 0 & 0 \\ 0 & 0 & 0 & 0 & 0 & 0 & N_i \\ 0 & 0 & 0 & 0 & 0 & N_i & 0 \end{bmatrix}$$

$$G_{bnli} = \begin{bmatrix} \frac{\partial N_i}{\partial x} & 0 & 0 & 0 & 0 & 0 & 0 \\ 0 & \frac{\partial N_i}{\partial y} & 0 & 0 & 0 & 0 & 0 \\ 0 & 0 & \frac{\partial N_i}{\partial x} & 0 & 0 & 0 & 0 \\ \frac{\partial N_i}{\partial y} & 0 & 0 & 0 & 0 & 0 & 0 \\ 0 & \frac{\partial N_i}{\partial x} & 0 & 0 & 0 & 0 & 0 \\ 0 & 0 & \frac{\partial N_i}{\partial y} & 0 & 0 & 0 & 0 \\ 0 & 0 & 0 & \frac{\partial N_i}{\partial x} & 0 & 0 & 0 \\ 0 & 0 & 0 & 0 & \frac{\partial N_i}{\partial y} & 0 & 0 \\ 0 & 0 & 0 & 0 & 0 & \frac{\partial N_i}{\partial x} & 0 \\ 0 & 0 & 0 & 0 & 0 & 0 & \frac{\partial N_i}{\partial y} \\ 0 & 0 & 0 & 0 & \frac{\partial N_i}{\partial x} & 0 & 0 \\ 0 & 0 & 0 & 0 & 0 & 0 & \frac{\partial N_i}{\partial y} \\ 0 & 0 & 0 & 0 & 0 & \frac{\partial N_i}{\partial y} & 0 \\ 0 & 0 & 0 & 0 & 0 & 0 & \frac{\partial N_i}{\partial x} \\ 0 & 0 & 0 & 0 & 0 & \frac{\partial N_i}{\partial y} & 0 \\ 0 & 0 & 0 & 0 & 0 & 0 & N_i \\ 0 & 0 & 0 & 0 & 0 & N_i & 0 \\ 0 & 0 & 0 & 0 & 0 & 0 & N_i \\ 0 & 0 & 0 & 0 & 0 & 0 & N_i \end{bmatrix}$$

$$G_{snli} = \begin{bmatrix} \frac{\partial N_i}{\partial x} & 0 & 0 & 0 & 0 & 0 & 0 \\ \frac{\partial N_i}{\partial y} & 0 & 0 & 0 & 0 & 0 & 0 \\ 0 & \frac{\partial N_i}{\partial x} & 0 & 0 & 0 & 0 & 0 \\ 0 & \frac{\partial N_i}{\partial y} & 0 & 0 & 0 & 0 & 0 \\ 0 & 0 & 0 & \frac{\partial N_i}{\partial x} & 0 & 0 & 0 \\ 0 & 0 & 0 & 0 & \frac{\partial N_i}{\partial y} & 0 & 0 \\ 0 & 0 & 0 & 0 & 0 & \frac{\partial N_i}{\partial x} & 0 \\ 0 & 0 & 0 & 0 & 0 & 0 & \frac{\partial N_i}{\partial y} \\ 0 & 0 & 0 & 0 & 0 & 0 & 0 \\ 0 & 0 & 0 & 0 & 0 & 0 & \frac{\partial N_i}{\partial x} \\ 0 & 0 & 0 & 0 & 0 & 0 & \frac{\partial N_i}{\partial y} \\ 0 & 0 & 0 & 0 & 0 & \frac{\partial N_i}{\partial x} & 0 \\ 0 & 0 & 0 & 0 & 0 & 0 & \frac{\partial N_i}{\partial y} \\ 0 & 0 & 0 & 0 & 0 & 0 & N_i \\ 0 & 0 & 0 & 0 & 0 & N_i & 0 \\ 0 & 0 & 0 & 0 & 0 & 0 & N_i \\ 0 & 0 & 0 & 0 & 0 & 0 & N_i \end{bmatrix}$$

Appendix D. The expression of S_b and S_s

$$S_b = \begin{bmatrix} N_x & 0 & 0 & N_{xy} & 0 & 0 & M_x & M_{xy} & 0 & 0 & P_x & P_{xy} & 0 & 0 \\ 0 & N_x & 0 & 0 & N_{xy} & 0 & 0 & 0 & M_x & M_{xy} & 0 & 0 & P_x & P_{xy} \\ 0 & 0 & N_x & 0 & 0 & N_{xy} & 0 & 0 & 0 & 0 & 0 & 0 & 0 & 0 \\ N_{xy} & 0 & 0 & N_y & 0 & 0 & M_{xy} & M_y & 0 & 0 & P_{xy} & P_y & 0 & 0 \\ 0 & N_{xy} & 0 & 0 & N_y & 0 & 0 & 0 & M_{xy} & M_y & 0 & 0 & P_{xy} & P_y \\ 0 & 0 & N_{xy} & 0 & 0 & N_y & 0 & 0 & 0 & 0 & 0 & 0 & 0 & 0 \\ M_x & 0 & 0 & M_{xy} & 0 & 0 & L_x & L_{xy} & 0 & 0 & R_x & R_{xy} & 0 & 0 \\ M_{xy} & 0 & 0 & M_y & 0 & 0 & L_{xy} & L_y & 0 & 0 & R_{xy} & R_y & 0 & 0 \\ 0 & M_x & 0 & 0 & M_{xy} & 0 & 0 & 0 & L_x & L_{xy} & 0 & 0 & R_x & R_{xy} \\ 0 & M_{xy} & 0 & 0 & M_y & 0 & 0 & 0 & L_{xy} & L_y & 0 & 0 & R_{xy} & R_y \\ P_x & 0 & 0 & P_{xy} & 0 & 0 & R_x & R_{xy} & 0 & 0 & V_x & V_{xy} & 0 & 0 \\ P_{xy} & 0 & 0 & P_y & 0 & 0 & R_{xy} & R_y & 0 & 0 & V_{xy} & V_y & 0 & 0 \\ 0 & P_x & 0 & 0 & P_{xy} & 0 & 0 & 0 & R_x & R_{xy} & 0 & 0 & V_x & V_{xy} \\ 0 & P_{xy} & 0 & 0 & P_y & 0 & 0 & 0 & R_{xy} & R_y & 0 & 0 & V_{xy} & V_y \end{bmatrix}$$

$$S_s = \begin{bmatrix} 0 & 0 & 0 & 0 & 0 & 0 & 0 & 0 & 0 & 0 & 0 & N_{xz} & 0 & R_{xz} & 0 \\ 0 & 0 & 0 & 0 & 0 & 0 & 0 & 0 & 0 & 0 & 0 & N_{yz} & 0 & R_{yz} & 0 \\ 0 & 0 & 0 & 0 & 0 & 0 & 0 & 0 & 0 & 0 & 0 & 0 & N_{xz} & 0 & R_{xz} \\ 0 & 0 & 0 & 0 & 0 & 0 & 0 & 0 & 0 & 0 & 0 & 0 & N_{yz} & 0 & R_{yz} \\ 0 & 0 & 0 & 0 & 0 & 0 & 0 & 0 & 0 & 0 & 0 & 0 & M_{xz} & 0 & L_{xz} \\ 0 & 0 & 0 & 0 & 0 & 0 & 0 & 0 & 0 & 0 & 0 & 0 & M_{yz} & 0 & L_{yz} \\ 0 & 0 & 0 & 0 & 0 & 0 & 0 & 0 & 0 & 0 & 0 & 0 & 0 & M_{xz} & 0 & L_{xz} \\ 0 & 0 & 0 & 0 & 0 & 0 & 0 & 0 & 0 & 0 & 0 & 0 & 0 & M_{yz} & 0 & L_{yz} \\ 0 & 0 & 0 & 0 & 0 & 0 & 0 & 0 & 0 & 0 & 0 & 0 & P_{xz} & 0 & V_{xz} \\ 0 & 0 & 0 & 0 & 0 & 0 & 0 & 0 & 0 & 0 & 0 & 0 & P_{yz} & 0 & V_{yz} \\ 0 & 0 & 0 & 0 & 0 & 0 & 0 & 0 & 0 & 0 & 0 & 0 & 0 & P_{xz} & 0 & V_{xz} \\ 0 & 0 & 0 & 0 & 0 & 0 & 0 & 0 & 0 & 0 & 0 & 0 & 0 & P_{yz} & 0 & V_{yz} \\ N_{xz} & N_{yz} & 0 & 0 & M_{xz} & M_{yz} & 0 & 0 & P_{xz} & P_{yz} & 0 & 0 & 0 & 0 & 0 & 0 \\ 0 & 0 & N_{xz} & N_{yz} & 0 & 0 & M_{xz} & M_{yz} & 0 & 0 & P_{xz} & P_{yz} & 0 & 0 & 0 & 0 \\ R_{xz} & R_{yz} & 0 & 0 & L_{xz} & L_{yz} & 0 & 0 & V_{xz} & V_{yz} & 0 & 0 & 0 & 0 & 0 & 0 \\ 0 & 0 & R_{xz} & R_{yz} & 0 & 0 & L_{xz} & L_{yz} & 0 & 0 & V_{xz} & V_{yz} & 0 & 0 & 0 & 0 \end{bmatrix}$$

References

- [1] Ghugal Y, Shimpi R. A review of refined shear deformation theories of isotropic and anisotropic laminated plates. *J Reinforced Plast Compos* 2002;21(9):775–813. <https://doi.org/10.1177/07316840212898841>.
- [2] Sayyad AS, Ghugal YM. On the free vibration analysis of laminated composite and sandwich plates: A review of recent literature with some numerical results. *Compos Struct* 2015;129:177–201. <https://doi.org/10.1016/j.compositstruct.2015.04.007>.
- [3] Gupta A, Ghosh A. Isogeometric static and dynamic analysis of laminated and sandwich composite plates using nonpolynomial shear deformation theory. *Compos Part B* 2019;176:. <https://doi.org/10.1016/j.compositesb.2019.107295>.
- [4] Thakur BR, Verma S, Singh B, Maiti D. Geometrically nonlinear dynamic analysis of laminated composite plate using a nonpolynomial shear deformation theory. *Int J Non-Linear Mech* 2020;. <https://doi.org/10.1016/j.ijnonlinmec.2020.103635>.
- [5] Zenkour AM. Hygrothermal effects on the bending of angle-ply composite plates using a sinusoidal theory. *Compos Struct* 2012;94(12):3685–96. <https://doi.org/10.1016/j.compositstruct.2012.05.033>.
- [6] Ramos I, Mantari J, Zenkour A. Laminated composite plates subject to thermal load using trigonometrical theory based on Carrera unified formulation. *Compos Struct* 2016;143:324–35. <https://doi.org/10.1016/j.compositstruct.2016.02.020>.
- [7] Garg N, Karkhanis RS, Sahoo R, Maiti P, Singh B. Trigonometric zigzag theory for static analysis of laminated composite and sandwich plates under hydro-thermo-mechanical loading. *Compos Struct* 2019;209:460–71. <https://doi.org/10.1016/j.compositstruct.2018.10.064>.
- [8] Abrate S, Sciuva MD. Equivalent single layer theories for composite and sandwich structures: A review. *Compos Struct* 2017;179:482–94. <https://doi.org/10.1016/j.compositstruct.2017.07.090>.
- [9] Whitney J, Ashton J. Effect of environment on the elastic response of layered composite plates. *AIAA J* 1971;9(9):1708–13. <https://doi.org/10.2514/3.49976>.
- [10] Adams DF, Miller AK. Hygrothermal microstresses in a unidirectional composite exhibiting inelastic material behavior. *J Compos Mater* 1977;11(3):285–99. <https://doi.org/10.1177/002199837701100304>.
- [11] Pipes RB, Vinson JR, Chou T-W. On the hygrothermal response of laminated composite systems. *J Compos Mater* 1976;10(2):129–48. <https://doi.org/10.1177/002199837601000203>.
- [12] Ram KS, Sinha P. Hygrothermal effects on the bending characteristics of laminated composite plates. *Comput Struct* 1991;40(4):1009–15. [https://doi.org/10.1016/0045-7949\(91\)90332-g](https://doi.org/10.1016/0045-7949(91)90332-g).
- [13] Ram KS, Sinha P. Hygrothermal effects on the free vibration of laminated composite plates. *J Sound Vib* 1992;158(1):133–48. [https://doi.org/10.1016/0022-460x\(92\)90669-a](https://doi.org/10.1016/0022-460x(92)90669-a).
- [14] Mukherjee N, Sinha P. Three-dimensional thermo-structural analysis of multidirectional fibrous composite plates. *Compos Struct* 1994;28(3):333–46. [https://doi.org/10.1016/0263-8223\(94\)90020-5](https://doi.org/10.1016/0263-8223(94)90020-5).
- [15] Parhi P, Bhattacharya S, Sinha P. Hygrothermal effects on the dynamic behavior of multiple delaminated composite plates and shells. *J Sound Vib* 2001;248(2):195–214. <https://doi.org/10.1006/jsvi.2000.3506>.
- [16] Natarajan S, Deogekar PS, Manickam G, Belouettar S. Hygrothermal effects on the free vibration and buckling of laminated composites with cutouts. *Compos Struct* 2014;108:848–55. <https://doi.org/10.1016/j.compositstruct.2013.10.009>.
- [17] Zhang H, Zhu R, Shi D, Wang Q. A simplified plate theory for vibration analysis of composite laminated sector, annular and circular plate. *Thin-Wall Struct* 2019;143:. <https://doi.org/10.1016/j.tws.2019.106252>.
- [18] Patel B, Ganapathi M, Makhecha D. Hygrothermal effects on the structural behaviour of thick composite laminates using higher-order theory. *Compos Struct* 2002;56(1):25–34. [https://doi.org/10.1016/s0263-8223\(01\)00182-9](https://doi.org/10.1016/s0263-8223(01)00182-9).
- [19] Shen H-S, Zheng J-J, Huang X-L. Dynamic response of shear deformable laminated plates under thermomechanical loading and resting on elastic foundations.

- Compos Struct 2003;60(1):57–66. [https://doi.org/10.1016/s0263-8223\(02\)00295-7](https://doi.org/10.1016/s0263-8223(02)00295-7).
- [20] Bahrami A, Nosier A. Interlaminar hydrothermal stresses in laminated plates. Int J Solids Struct 2007;44(25–26):8119–42. <https://doi.org/10.1016/j.ijsolstr.2007.06.004>.
- [21] Lo S, Zhen W, Cheung Y, Wanji C. Hydrothermal effects on multilayered composite plates using a refined higher order theory. Compos Struct 2010;92(3):633–46. <https://doi.org/10.1016/j.compstruct.2009.09.034>.
- [22] Zhao R, Yu K, Hulbert GM, Wu Y, Li X. Piecewise shear deformation theory and finite element formulation for vibration analysis of laminated composite and sandwich plates in thermal environments. Compos Struct 2017;160:1060–83. <https://doi.org/10.1016/j.compstruct.2016.10.103>.
- [23] Zenkour AM. Bending of thin rectangular plates with variable-thickness in a hydrothermal environment. Thin-Wall Struct 2018;123:333–40. <https://doi.org/10.1016/j.tws.2017.11.038>.
- [24] Vinyas M, Kattimani SC. Finite element evaluation of free vibration characteristics of magneto-electro-elastic rectangular plates in hydrothermal environment using higher-order shear deformation theory. Compos Struct 2018;202:1339–52. <https://doi.org/10.1016/j.compstruct.2018.06.069>.
- [25] Carrera E. An assessment of mixed and classical theories for the thermal stress analysis of orthotropic multilayered plates. J Therm Stress 2000;23(9):797–831. <https://doi.org/10.1080/014957300750040096>.
- [26] Rao V, Sinha P. Dynamic response of multidirectional composites in hydrothermal environments. Compos Struct 2004;64(3–4):329–38. <https://doi.org/10.1016/j.compstruct.2003.09.002>.
- [27] Jin Q, Yao W. Hydrothermal analysis of laminated composite plates in terms of an improved c0-type global-local model. Aerosp Sci Technol 2017;63:328–43. <https://doi.org/10.1016/j.ast.2017.01.004>.
- [28] Benkhenda A, Tounsi A, et al. Effect of temperature and humidity on transient hydrothermal stresses during moisture desorption in laminated composite plates. Compos Struct 2008;82(4):629–35. <https://doi.org/10.1016/j.compstruct.2007.04.013>.
- [29] Yifeng Z, Yu W. A variational asymptotic approach for hydrothermal analysis of composite laminates. Compos Struct 2011;93(12):3229–38. <https://doi.org/10.1016/j.compstruct.2011.06.003>.
- [30] Amoushahi H, Goodarzian F. Dynamic and buckling analysis of composite laminated plates with and without strip delamination under hydrothermal effects using finite strip method. Thin-Wall Struct 2018;131:88–101. <https://doi.org/10.1016/j.tws.2018.06.030>.
- [31] Wang L, Chen T. Structural intensity analysis of the cantilevered plate under thermal load. Thin-Wall Struct 2019;139:209–18. <https://doi.org/10.1016/j.tws.2019.03.012>.
- [32] Moleiro F, Carrera E, Ferreira A, Reddy J. Hygro-thermo-mechanical modelling and analysis of multilayered plates with embedded functionally graded material layers. Compos Struct 2020;233:. <https://doi.org/10.1016/j.compstruct.2019.111442>.
- [33] Cheng M, Zhong Y, Kureemun U, Cao D, Hu H, Lee HP, Li S. Environmental durability of carbon/flax fiber hybrid composites. Compos Struct 2020;234:. <https://doi.org/10.1016/j.compstruct.2019.111719>.
- [34] Garg A, Chalak H. A review on analysis of laminated composite and sandwich structures under hydrothermal conditions. Thin-Wall Struct 2019;142:205–26. <https://doi.org/10.1016/j.tws.2019.05.005>.
- [35] Sit M, Ray C. A third order nonlinear model to study the dynamic behaviour of composite laminated structures under thermal effect with experimental verification. Compos Struct 2019;212:106–17. <https://doi.org/10.1016/j.compstruct.2019.01.012>.
- [36] Zhong Y, Cheng M, Zhang X, Hu H, Cao D, Li S. Hydrothermal durability of glass and carbon fiber reinforced composites—a comparative study. Compos Struct 2019;211:134–43. <https://doi.org/10.1016/j.compstruct.2018.12.034>.
- [37] Moleiro F, Soares CM, Carrera E. Three-dimensional exact hydro-thermo-elastic solutions for multilayered plates: Composite laminates, fibre metal laminates and sandwich plates. Compos Struct 2019;216:260–78. <https://doi.org/10.1016/j.compstruct.2019.02.071>.
- [38] Feng Y, Ma B, Cui R, An T, He Y, Jiao S. Effects of hydrothermal environment on the buckling and postbuckling performances of stiffened composite panels under axial compression. Compos Struct 2020;. <https://doi.org/10.1016/j.compstruct.2020.112123>.
- [39] Pividialyk I, Rozycski P, Jacquemin F, Gornet L, Auger S. Experimental analysis of the mechanical performance of glass fibre reinforced 6 under varying environmental conditions. Compos Struct 2020;. <https://doi.org/10.1016/j.compstruct.2020.112338>.
- [40] Zabaras N, Pervez T. Viscous damping approximation of laminated anisotropic composite plates using the finite element method. Comput Meth Appl Mech Eng 1990;81(3):291–316. [https://doi.org/10.1016/0045-7825\(90\)90058-1](https://doi.org/10.1016/0045-7825(90)90058-1).
- [41] Pervez T, Zabaras N. Transient dynamic and damping analysis of laminated anisotropic plates using a refined plate theory. Int J Numer Meth Eng 1992;33(5):1059–80. <https://doi.org/10.1002/nme.1620330511>.
- [42] Latheswary S, Valsarajan K, Sadasiva Rao Y. Dynamic response of moderately thick composite plates. Journal of Sound Vibration 2004;270:417–26. [https://doi.org/10.1016/s0022-460x\(03\)00511-x](https://doi.org/10.1016/s0022-460x(03)00511-x).
- [43] Assaei H, Pournoori N. Development of a viscoelastic spline finite strip formulation for transient analysis of plates. Thin-Wall Struct 2018;124:430–6. <https://doi.org/10.1016/j.tws.2017.12.021>.
- [44] Pap ZB, Kollár LP. Dynamic response of long rectangular floors subjected to periodic force excitation. Materials 2019;12(9):1417. <https://doi.org/10.3390/ma12091417>.
- [45] Zhang C, Jin G, Ye T, Zhang Y. Harmonic response analysis of coupled plate structures using the dynamic stiffness method. Thin-Wall Struct 2018;127:402–15. <https://doi.org/10.1016/j.tws.2018.02.014>.
- [46] Aljani F, Bakhtiari-Nejad F, Amabili M. Nonlinear vibrations of fgm rectangular plates in thermal environments. Nonlinear Dyn 2011;66(3):251. <https://doi.org/10.1007/s11071-011-0049-8>.
- [47] J. Goldberg, H. Leve, Theory of prismatic folded plate structures, int, Association for Bridge and Structural Engineering J 17..
- [48] Irie T, Yamada G, Kobayashi Y. Free vibration of a cantilever folded plate. J Acoust Soc Am 1984;76(6):1743–8. <https://doi.org/10.1121/1.391622>.
- [49] Guha Niogi A, Laha M, Sinha P. Finite element vibration analysis of laminated composite folded plate structures. Shock Vib 1999;6(5–6):273–83. <https://doi.org/10.1155/1999/354234>.
- [50] Lee S-Y, Wooh S-C, Yhim S-S. Dynamic behavior of folded composite plates analyzed by the third order plate theory. Int J Solids Struct 2004;41(7):1879–92. <https://doi.org/10.1016/j.ijsolstr.2003.11.026>.
- [51] Lee S-Y, Wooh S-C. Finite element vibration analysis of composite box structures using the high order plate theory. J Sound Vib 2004;277(4–5):801–14. <https://doi.org/10.1016/j.jsv.2003.09.024>.
- [52] Haldar S, Sheikh AH. Free vibration analysis of isotropic and composite folded plates using a shear flexible element. Finite Elem Anal Des 2005;42(3):208–26. <https://doi.org/10.1016/j.finel.2005.06.003>.
- [53] Daniel A, Doyle J, Rizzi S. Dynamic analysis of folded plate structures. J Vib Acoust 1996;118(4):591–8. <https://doi.org/10.1115/1.2888339>.
- [54] Golley BW, Grice WA. Prismatic folded plate analysis using finite strip-elements. Comput Methods Appl Mech Eng 1989;76(2):101–18. [https://doi.org/10.1016/0045-7825\(89\)90090-x](https://doi.org/10.1016/0045-7825(89)90090-x).
- [55] Eterovic AL, Godoy LA. An exact strip method for folded plate structures. Comput Struct 1988;32(2):263–76. [https://doi.org/10.1016/0045-7949\(89\)90038-2](https://doi.org/10.1016/0045-7949(89)90038-2).
- [56] Bandyopadhyay J, Laad P. Comparative analysis of folded plate structures. Comput Struct 1990;36(2):291–6. [https://doi.org/10.1016/0045-7949\(90\)90128-o](https://doi.org/10.1016/0045-7949(90)90128-o).
- [57] Ohga M, Shigematsu T. Bending analysis of plates with variable thickness by boundary element-transfer matrix method. Comput Struct 1988;28(5):635–40. [https://doi.org/10.1016/0045-7949\(88\)90008-9](https://doi.org/10.1016/0045-7949(88)90008-9).
- [58] Ohga M, Shigematsu T, Kohigashi S. Analysis of folded plate structures by a combined boundary element-transfer matrix method. Comput Struct 1991;41(4):739–44. [https://doi.org/10.1016/0045-7949\(91\)90183-m](https://doi.org/10.1016/0045-7949(91)90183-m).
- [59] Liu W, Huang C. Vibration analysis of folded plates. J Sound Vib 1992;157(1):123–37. [https://doi.org/10.1016/0022-460x\(92\)90570-n](https://doi.org/10.1016/0022-460x(92)90570-n).
- [60] Duan M, Miyamoto Y. Effective hybrid/mixed finite elements for folded-plate structures. J Eng Mech 2002;128(2):202–8. [https://doi.org/10.1061/\(ASCE\)0733-9399\(2002\)128:2\(202\)](https://doi.org/10.1061/(ASCE)0733-9399(2002)128:2(202)).
- [61] Schlothauer A, Fasel U, Keidel D, Ermanni P. High load carrying structures made from folded composite materials. Compos Struct 2020;250:. <https://doi.org/10.1016/j.compstruct.2020.112612>.
- [62] Le-Anh L, Nguyen-Thoi T, Ho-Huu V, Dang-Trung H, Bui-Xuan T. Static and frequency optimization of folded laminated composite plates using an adjusted differential evolution algorithm and a smoothed triangular plate element. Compos Struct 2015;127:382–94. <https://doi.org/10.1016/j.compstruct.2015.02.069>.
- [63] Wang Z, Zhou C, Khalilov V, Shabalov A. An experimental study on the radar absorbing characteristics of folded core structures. Compos Struct 2018;194:199–207. <https://doi.org/10.1016/j.compstruct.2018.03.106>.
- [64] Xiang X, You Z, Lu G. Rectangular sandwich plates with miura-ori folded core under quasi-static loadings. Compos Struct 2018;195:359–74. <https://doi.org/10.1016/j.compstruct.2018.04.084>.
- [65] Ye H, Ma J, Zhou X, Wang H, You Z. Energy absorption behaviors of pre-folded composite tubes with the full-diamond origami patterns. Compos Struct 2019;221:. <https://doi.org/10.1016/j.compstruct.2019.110904>.
- [66] Mader A, Born L, Körner A, Schieber G, Masset P-A, Milwich M, Gresser GT, Knippers J. Bio-inspired integrated pneumatic actuation for compliant fiber-reinforced plastics. Compos Struct 2020;233:. <https://doi.org/10.1016/j.compstruct.2019.111558>.
- [67] Thakur BR, Verma S, Singh B, Maiti D. Dynamic analysis of folded laminated composite plate using nonpolynomial shear deformation theory. Aerosp Sci Technol 2020;. <https://doi.org/10.1016/j.ast.2020.106083>.
- [68] Das S, Niogi AG. Free-vibration analysis of epoxy-based cross-ply laminated composite folded plates subjected to hydro-thermal loading. J Inst Eng (India): Series C 2020;101(3):541–557. doi:10.1007/s40032-020-00573-8..
- [69] Grover N, Singh B, Maiti D. New nonpolynomial shear-deformation theories for structural behavior of laminated-composite and sandwich plates. AIAA J 2013;51(8):1861–71. <https://doi.org/10.2514/1.j052399>.
- [70] Verma S, Thakur BR, Singh B, Maiti D. Aerosp Sci Technol 2021;112:. <https://doi.org/10.1016/j.ast.2021.106635>.
- [71] Reddy JN. Mechanics of laminated composite plates and shells. CRC Press 2004. <https://doi.org/10.1201/b12409>.
- [72] Caughey T, O'Kelly ME. Classical normal modes in damped linear dynamic systems. J Appl Mech 1965;32(3):583–588. doi:10.1115/1.3643949..
- [73] Kj B. Finite element procedures in engineering analysis, 1982.
- [74] Grover N, Singh B, Maiti D. Int J Mech Sci 2013;67:89–99. <https://doi.org/10.1016/j.ijmecsci.2012.12.010>.
- [75] Noor AK. Free vibrations of multilayered composite plates. AIAA J 1973;11(7):1038–9. <https://doi.org/10.2514/3.6868>.
- [76] Huang X-L, Shen H-S, Zheng J-J. Nonlinear vibration and dynamic response of shear deformable laminated plates in hydrothermal environments. Compos Sci Technol 2004;64(10–11):1419–35. <https://doi.org/10.1016/j.compscitech.2003.09.028>.